On the ~~Contribution~~ contribution of ~~Grain Boundary Sliding~~ grain boundary sliding type creep to ~~Firn Densification -~~ firn densification ~~–~~ an ~~Assessment~~ assessment using an ~~Optimisation Approach~~optimization approach

Timm Schultz[1], Ralf Müller[1], Dietmar Gross[2], and Angelika Humbert[3,4]

[1]Institute of Applied Mechanics, Technische Universität Kaiserslautern, Kaiserslautern, Germany
[2]Division of Solid Mechanics, Technische Universität Darmstadt, Darmstadt, Germany
[3]Alfred-Wegener-Institut Helmholtz-Zentrum für Polar- und Meeresforschung, Bremerhaven, Germany
[4]Faculty of Geosciences, University of Bremen, Bremen, Germany

Correspondence: Timm Schultz (tschultz@rhrk.uni-kl.de)

Abstract. ~~Physics based simulation~~ Simulation approaches to firn densification often rely on the assumption that grain boundary sliding is the leading process driving the first stage of densification. Alley (1987) first developed a ~~material model for firn describing~~ process-based material model of firn that describes this process. However, often ~~so called semi empirical~~ so-called semi-empirical models are favored ~~against the~~ over the physical description of grain boundary sliding ~~due to simplicity and~~ owing to their simplicity and the uncertainties regarding model parameters. In this study, we ~~are assessing~~ assessed the applicability of the grain boundary sliding model of Alley (1987) to firn using a numeric firn densification model and an ~~optimisation~~ optimization approach, for which we ~~formulate~~ formulated variants of the constitutive relation ~~by~~ of Alley (1987). ~~The~~ An efficient model implementation based on an updated Lagrangian numerical scheme ~~enables~~ enabled us to perform a large number of simulations ~~testing~~ to test different model parameters ~~, to find simulation results suiting~~ and identify the simulation results that best reproduced 159 firn density profiles from Greenland and Antarctica~~best~~. For most of the investigated locations~~a good agreement of~~ , the simulated and measured firn density profiles ~~was found. This~~ were in good agreement. This result implies that the constitutive relation ~~by~~ of Alley (1987) ~~characterises~~ characterizes the first stage of firn densification well ~~, if suitable model parameter~~ when suitable model parameters are used. An analysis of the parameters that ~~lead to best matches reveals a dependency~~ result in the best agreement revealed a dependence on the mean surface mass balance. This ~~may indicate an insufficient description of the load situation, as~~ finding may indicate that the load is insufficiently described, as the lateral components of the stress tensor are usually neglected in ~~one dimensional~~ one-dimensional models of the firn column.

1 Introduction

~~Two basic categories of firn densification models can be identified. The first one, incorporating the majority of~~ Firn densification models fall into two basic categories. Models in the first category, which includes most existing models, ~~is following the so called semi empirical concept~~ follow the so-called semi-empirical approach of Herron and Langway (1980), which itself is based on Sorge's Law (Bader, 1954) and the Robin ~~Hypothesis~~ hypothesis (Robin, 1958). Examples are the models ~~by~~ of Arthern et al. (2010), Ligtenberg et al. (2011), and Simonsen et al. (2013). ~~Typically~~ The empirical parameters of these models are ~~adjusted to~~ typically adjusted on the basis of certain datasets of depth density profiles. ~~The~~ In the second category of firn densification models~~tries~~ , an attempt is made to quantify the physical processes related to ~~the densification of firn~~ firn densification. These processes ~~incorporate different~~ include various types of creep and diffusion. ~~Micro mechanical~~ Micromechanical models are used for ~~small scale~~ small-scale investigations (Johnson and Hopkins, 2005; Theile et al., 2011; Fourtenau et al., 2020)~~while continuum mechanics based models~~ , whereas models based on continuum mechanics can be used for ~~large scale~~ large-scale simulations. Examples of the latter are ~~models by~~ the models of Arthern and Wingham (1998), Arnaud et al. (2000), and Goujon et al. (2003).

Alley (1987) first applied the theory of grain boundary sliding ~~,~~ adopted from Raj and Ashby (1971) ~~,~~ to firn densification at densities below the critical density of $\rho_c = 550\,\mathrm{kg\,m^{-3}}$. ~~Since then the~~ The description of this process by Alley (1987) was subsequently used in other firn densification models (Arthern and Wingham, 1998; Arnaud et al., 2000; Goujon et al., 2003; Bréant et al., 2017). ~~Nevertheless~~However, the assumption that grain boundary sliding is the dominant process in firn densification at densities below $\rho_c = 550\,\mathrm{kg\,m^{-3}}$ ~~was~~ has been questioned numerous times (Ignat and Frost, 1987; Roscoat et al., 2010). For example~~, by conducting ,~~ Theile et al. (2011) conducted experiments on a small number of snow samples ~~, suggested that the~~ and suggested that densification is more likely driven by processes within the grain rather than by the ~~inter granular~~ intergranular process of grain boundary sliding.

~~When first published the description of grain boundary sliding for firn, he tested the material model by fitting the model results to four firn profiles available at this time, evaluating the resulting model parameters. As indicated by the title of his paper and pointed out in its discussion, grain boundary sliding might not be the only process driving the densification of firn at low density and model parameters might differ, but by using the given constitutive law it is possible to reproduce measured depth density profiles to a satisfying degree.~~

In this study~~we aim at evaluating:~~ , we aim to evaluate (i) whether the description of grain boundary sliding ~~and its description~~ given by Alley (1987) is suitable for the simulation of firn densification at low density, (ii) how a modification of the constitutive relation introduced by Bréant et al. (2017) affects simulation results, (iii) ~~if~~ whether hidden or additional dependencies ~~of the constitutive relation~~ on climatic or other conditions can be identified in the constitutive relation, and (iv) how ~~a modification of~~ the constitutive relation ~~by~~ of Alley (1987) ~~, leading to improvement of the description, could look like. We want to point out~~ might be improved. Note that our study aims ~~at assessing~~ to assess the constitutive relation for grain boundary sliding proposed by Alley (1987). An evaluation ~~clarifying if~~ that clarifies whether grain boundary sliding is the ~~dominating~~ dominant process driving firn densification below the critical density of $\rho_c = 550\,\mathrm{kg\,m^{-3}}$ ~~has to be carried out~~ must be conducted using other methods. ~~Attempts~~ Experimental attempts to do so have been made ~~for example by~~ by, for example, Kinosita (1967), Ignat and Frost (1987), and Theile et al. (2011)~~by conducting experiments~~. In contrast to these experimental investigations~~we follow a~~

~~combination of data and physical model based approach~~ , a data-driven model approach is used in our study. Since the original study ~~by~~ of Alley (1987) was published, the amount of available data ~~became much larger. Alongside to~~ has increased greatly. The data include a large number of firn profiles ~~this includes forcing datawhich, together with additional modelling techniques, allows~~ and forcing data, and they allow us to simulate firn profiles at ~~a~~ very high quality using additional modeling techniques.

2 Methods

~~In order to~~ To test the description of grain boundary sliding given by Alley (1987)~~we use a numeric model , simulating~~ , we used a numerical model to simulate the evolution of a ~~one dimensional~~ one-dimensional firn column with ~~respect to~~ time. The model ~~incorporates~~ uses variants of the constitutive relation of Alley (1987), all of which combine several model parameters in a single factor. We ~~then~~ force the model with data provided by the regional climate model RACMO2.3 (Van Wessem et al., 2014; Noël et al., 2015), ~~representing~~ which represents the climate of ~~the last~~ recent decades at 159 ~~different~~ locations where firn density measurements were ~~retrieved~~made. These firn measurements are available through the ~~"~~Surface Mass Balance and Snow Depth on Sea Ice Working Group (SUMup) snow density subdataset ~~"~~ (Koenig and Montgomery, 2019). By varying the factor ~~incorporated~~ used in the variants of the constitutive equation, we ~~produce~~ produced a large number of simulation results, which ~~are~~ were compared to the corresponding density measurements. The quality of the factors used in the simulations ~~is evaluated by~~ was evaluated in terms of the deviation of the computed density profiles from the measured profiles. ~~Evaluating factor values leading to best results , reveals~~ The factor values that yielded the best results reveal possible improvements in the description of grain boundary sliding for firn densification at low density. In the following sections, the constitutive equation for grain boundary sliding given by Alley (1987), the ~~optimisation scheme~~optimization scheme, and the used density and forcing data are described. A detailed description of the model ~~can be found~~ is presented in the appendix (~~Section~~Sect. A).

2.1 ~~Grain Boundary Sliding~~Constitutive relation for grain boundary sliding

~~The different~~ We explain briefly the following components and characteristics of the constitutive law ~~by~~ of Alley (1987) describing the process of grain boundary sliding.

$$\dot{\varepsilon}_{zz} = -\frac{2}{15} \quad \delta_b \quad \frac{8\,D_{\mathrm{BD}}\Omega}{k_b T h^2} \quad \frac{1}{r\mu^2} \quad \left(\frac{\rho_{\mathrm{ice}}}{\rho}\right)^3 \quad \left(1 - \frac{5}{3}\frac{\rho}{\rho_{\mathrm{ice}}}\right) \quad \sigma_{zz} \quad , \qquad D_{\mathrm{BD}} = A_{\mathrm{BD}} \exp\left(-\frac{Q_{\mathrm{BD}}}{RT}\right) \tag{1}$$

~~will be explained briefly.~~ The factor of $2/15$ results from the geometric deviation pointed out by Alley (1987). Another geometric parameter, δ_b, describes the width of the grain boundary.

The following part of the equation describes the reciprocal bond or boundary viscosity (Raj and Ashby, 1971). The ~~optimisation~~ optimization approach of Alley (1987) ~~aimed to find optimal values for~~ was intended to identify the optimal values of the boundary viscosity. Alley (1987) compared the results ~~from this optimisation~~ of this optimization to the description of the boundary viscosity given by Raj and Ashby (1971), which ~~incorporates the factor D_{BD}, the~~ includes the volume of the H_2O molecule Ω, the Boltzmann constant k_b, the temperature T, and the amplitude of grain boundary obstructions, h. The latter is a measure ~~for~~ of the roughness of the grain boundary. D_{BD} is an Arrhenius ~~equation~~ factor describing the rate of boundary diffusion. Values

for the activation energy representative of the typical activation energy for this process, Q_{BD}, and the corresponding prefactor, A_{BD}, can be found in literature .the literature (e.g., Maeno and Ebinuma, 1983), and are further discussed in Sect. 2.2. R is the universal gas constant.

The strain rate resulting from grain boundary sliding also depends on the grain radius r. The ratio of the grain radius to the neck radius μ was introduced by Arthern and Wingham (1998) and is assumed to be constant. There are different methods Various methods can be used to determine the size of grains in crystalline materials (e.g., Gow, 1969). The model by of Alley (1987) was developed under the assumption of assuming perfectly spherical grains. Although this assumption is not true for firn, this assumption of firn, it provides a reasonable basis for modelling. Thereforemodeling. Therefore, throughout this paper, the grain radius r describes represents the radius of theoretical spherical grainsthroughout this study.

The next factor of Equationin Eq. (1) describes the dependency dependence on the inverse relative density to the power of threedensity relative to the ice density cubed. The factor of 5/3 corresponds to the inverse relative $1-(5\rho/3\rho_{\mathrm{ice}})$ causes the strain rate due to grain boundary sliding to decrease with increasing density until it vanishes at the critical density of $\rho_c = 550\,\mathrm{kg\,m^{-3}}$. When the critical density and with it the theoretical densest packing of spheres is reached, the maximum coordination number of a single grain is established . At this point grains can not close random packing is established (Anderson and Benson, 1963), and grains can no longer slide against each otherany more and ; thus, the process of grain boundary sliding ends. Other deformation processes, especially in particular dislocation creep (Maeno and Ebinuma, 1983), lead to result in further densification with increasing stress. This behaviour is achieved in the constitutive relation by the factor incorporating the relative density ρ/ρ_{ice}. The vertical strain rate $\dot{\epsilon}_{zz}$ decreases with increasing density ρ, until it becomes zero at the critical density ρ_c.

It has to be mentioned though, that

Alley (1987) suggested also other processes leading to densification act at densities that additional processes contribute to densification below the critical density. A decline of the strain rate due to It is feasible that the effect of grain boundary sliding while the influence on the strain rate decreases, whereas that of other processes increases, seems feasible. The studies by of Arthern and Wingham (1998) and Bréant et al. (2017) use this description, in which only grain boundary sliding driving the drives densification in the first stage of firn densificationexclusively. In the study by of Bréant et al. (2017), the constitutive relation by of Alley (1987) is changed in a way that leads to a modified such that the transition into the second stage of densification . We will is modified. We evaluate this modification throughout this studyin this work.

Finally, the stress in vertical directionthe vertical direction, σ_{zz}, resulting from the overburden firn is driving drives grain boundary sliding. While Whereas Alley (1987) used the product of the accumulation rate, acceleration due to gravity, and time since the deposition of a specific firn sample to describe the overburden stress, we use a more general form at this point (see Sectionhere [see Sect. A2, EquationEq. (A5))]. The other physical properties influencing affecting the process are density ρ, temperature T, and grain radius r.

2.2 ~~Optimisation~~Optimization

To test the ~~concept of the~~ material model developed by Alley (1987)~~we formulate variants of Equation~~, we formulated variants of Eq. (1) and ~~compare corresponding~~ compared the model results to density measurements of various firn cores. These variants of the constitutive equation ~~(Equations~~[Eqs. (2) to (5)~~)~~] preserve its general form ~~,~~ but group several material parameters into a single factor. ~~In this way~~ As a result, the simulation result does not depend on those parameters, but on the single factor. The factor is then varied to find an optimal simulation result ~~recreating~~ that best reproduces the measured firn profile~~best~~. The factor ~~leading to~~ that yields the optimal simulation result depends on the measured firn density profile and the corresponding climate conditions. It is therefore ~~site specific. This allows for the assessment if the~~ site-specific. This feature makes it possible to assess whether the description of grain boundary sliding given by Alley (1987) can be used to ~~recreate~~ reproduce measured firn profiles~~under the assumption of~~ , assuming an optimal set of parameters. It further allows ~~to analyse the site specific factors leading to~~ us to analyze the site-specific factors yielding the best simulation results for possible hidden dependencies.

Arnaud et al. (2000), Goujon et al. (2003)~~as well as~~ , and Bréant et al. (2017) also ~~summed~~ incorporated the material parameters of the model ~~by~~ of Alley (1987) ~~up~~ into a single parameter. ~~In the study by~~ Bréant et al. (2017) ~~additionally~~ also modified the factor of $5/3$ ~~was modified~~ to change the density at which the deformation due to grain boundary sliding becomes zero. In the following~~the~~ , four variants, indicated by the subscripts $(\cdot)_{\mathrm{v}_1}$ to $(\cdot)_{\mathrm{v}_4}$, are ~~shown~~presented:

$$\dot{\varepsilon}_{zz\,\mathrm{v}_1} = -C_{\mathrm{v}_1} D_{\mathrm{BD}} \frac{1}{T} \frac{1}{r} \left(\frac{\rho_{\mathrm{ice}}}{\rho}\right)^3 \left(1 - \frac{5}{3}\frac{\rho}{\rho_{\mathrm{ice}}}\right) \sigma_{zz} \quad , \qquad D_{\mathrm{BD}} = A_{\mathrm{BD}} \exp\left(-\frac{Q_{\mathrm{BD}}}{RT}\right) , \tag{2}$$

$$\dot{\varepsilon}_{zz\,\mathrm{v}_2} = -C_{\mathrm{v}_2} D_{\mathrm{BD}} \frac{1}{T} \frac{1}{r} \left(\frac{\rho_{\mathrm{ice}}}{\rho}\right)^3 \left(1 + \frac{0.5}{6} - \frac{5}{3}\frac{\rho}{\rho_{\mathrm{ice}}}\right) \sigma_{zz} \quad , \qquad D_{\mathrm{BD}} = A_{\mathrm{BD}} \exp\left(-\frac{Q_{\mathrm{BD}}}{RT}\right) . \tag{3}$$

Variant 1 ~~(Equation~~[Eq. (2)~~)~~] and Variant 2 ~~(Equation~~[Eq. (3)~~)~~] of the constitutive equation combine all material constants using the factors C_{v_1} and C_{v_2}, respectively. The Arrhenius ~~equation~~ factor for boundary diffusion, D_{BD}~~(see Equation~~, [see Eq. (1)~~) is preserved~~] is retained in these variants. Following Maeno and Ebinuma (1983), we use a value of $Q_{\mathrm{BD}} = 44.1\,\mathrm{kJ\,mol^{-1}}$ for the boundary diffusion activation energy. ~~It is~~ This variable was defined by Maeno and Ebinuma (1983) ~~by two thirds~~ as two-thirds of the activation energy for lattice diffusion measured by Itagaki (1964). The corresponding prefactor is $A_{\mathrm{BD}} = 3.0 \times 10^{-2}\,\mathrm{m^2\,s^{-}}$ Alley (1987) assumed a similar value for the boundary diffusion activation energy.

~~Except for~~ In addition to the temperature T, the vertical strain rate $\dot{\varepsilon}_{zz}$ ~~only depends~~ depends only on the firn density ρ, ~~the~~ grain radius r~~and the stress in~~ , and stress in the vertical direction σ_{zz}. Variant 2 differs from Variant 1 ~~by the use of the~~ in that it uses the modification introduced by Bréant et al. (2017). This modification ~~leads to a theoretical ending of~~ causes a theoretical end to the process of grain boundary sliding at ~~the~~ a density of $\rho_c^* = 596\,\mathrm{kg\,m^{-3}}$. It was introduced to ~~grant better transition into~~ obtain a better transition to the second stage of firn densification. The strain rate due to grain boundary sliding is therefore higher at the critical density when ~~using the modification~~ this modification of Bréant et al. (2017) is used.

To ~~test the influence~~ determine the effect of the Arrhenius ~~law~~ factor, it is disregarded in Variants 3 and 4, as shown in ~~Equations~~Eqs. (4) and (5):

$$\dot{\varepsilon}_{zz\,\mathrm{v}_3} = -C_{\mathrm{v}_3}\frac{1}{T}\frac{1}{r}\left(\frac{\rho_{\mathrm{ice}}}{\rho}\right)^3\left(1-\frac{5}{3}\frac{\rho}{\rho_{\mathrm{ice}}}\right)\sigma_{zz}\,, \tag{4}$$

$$\dot{\varepsilon}_{zz\,\mathrm{v}_4} = -C_{\mathrm{v}_4}\frac{1}{T}\frac{1}{r}\left(\frac{\rho_{\mathrm{ice}}}{\rho}\right)^3\left(1+\frac{0.5}{6}-\frac{5}{3}\frac{\rho}{\rho_{\mathrm{ice}}}\right)\sigma_{zz}\,. \tag{5}$$

~~Again in~~ In Variant 4~~the modification by~~, the modification of Bréant et al. (2017) is used~~while~~, whereas Variant 3 ~~incorporates~~ uses the original formulation ~~by~~ of Alley (1987).

~~The aim of the optimisation~~ The goal of optimization is to find optimal values of the factors C_{v} for every variant of the constitutive relation ~~(Equations~~[Eqs. (2) to (5)~~) resulting in a simulated density profile that represents~~] to produce simulated density profiles that best reproduce the measured profiles~~in the best possible way~~. As an example, we explain the ~~optimisation~~ optimization process for one selected firn core in more detail. The upper part of ice core ngt03C93.2 (Wilhelms, 2000) is shown in Fig. 1~~(a)~~a.

Every simulation ~~starts with a spin up~~ begins with a spin-up period in which constant values are used for ~~the forcing. When~~ forcing. The model is forced with prescribed values of temperature, accumulation rate, firn density, and grain radius at the surface. We check for steady-state conditions by comparing the change in density between time steps. If the maximum density change is smaller than $|\Delta\rho_{\mathrm{max}}| < 0.1\,\mathrm{kg\,m^{-3}}$, we assume that the steady state is reached. In this case, a transient run using ~~evolving~~ varying forcing data follows. We use a constant value of 48 time steps per year for spin-up and transient simulation runs (see Sect. A7). The forcing at the location of ngt03C93.2 is shown in Fig. 1~~(c)~~c. The resulting firn profile is then compared to the measured profile. We ~~use~~ used the root mean square deviation ~~between measured and modelled~~ (RMSD) between the measured and modeled density for comparison, ~~which allows a~~ as it is simple and easy to compute~~comparability between the simulation result and the density measurement~~. To calculate the deviation, the simulated density values are interpolated linearly to the measurement locations along the profile. To ~~guarantee a high~~ ensure the quality of the results, we ~~restrict~~ limited the calculation of the deviation to the domain defined by the the location of the uppermost available measurement point and the oldest simulated horizon within the firn profile affected by ~~the forcing. In case of~~ forcing. For ngt03C93.2, this horizon is the ~~surface of~~ 1958 surface at a depth of approximately $11\,\mathrm{m}$ below the surface, indicated by dashed horizontal lines in Fig. 1~~(a)~~a. Only results located above the ~~surface of~~ simulated 1958 surface are used to calculate the deviation. The reason is that the forcing data from RACMO2.3 (Van Wessem et al., 2014; Noël et al., 2015) begin in 1958 ~~are incorporated in the calculation of the deviation. Examining~~ for Greenland. Consequently, the results are not affected by the spin-up period. For firn profiles retrieved in Antarctica, climate forcing from RACMO2.3 begins in 1979. Thus, only those results located above the simulated horizon of 1979 are considered for comparison with the Antarctic firn profiles. The examination of other firn cores ~~,~~ revealed that the surface of the oldest available forcing may be located at greater depth ~~, when a~~ when the density of $\rho_c = 550\,\mathrm{kg\,m^{-3}}$ ~~is already~~ has already been reached. In those cases, the computation of the ~~root mean square deviation is restricted~~ RMSD was limited to the domain showing density values ~~smaller than~~ below $540\,\mathrm{kg\,m^{-3}}$. We decided to use a ~~smaller density threshold~~

than density threshold below the critical density due to the asymptotic characteristic because of the asymptotic nature of the resulting density profiles obtained using Variants 1 and 3 of the constitutive equation (Equations[Eqs. (2) and (4)]). The value of $540\,\mathrm{kg\,m^{-3}}$ rendered to ensure comparability between results of the different was chosen to ensure that the results obtained using the variants of the constitutive relation while unique values for the factorsare comparable, whereas unique values of the factor C_v were found quickly throughout the optimisationquickly determined throughout the optimization.

As the implementation of our model is efficient and the approach is as well simple and reliable, we decided to determine the best factor C_v for the four variants of the constitutive equation , by simply testing 250 values within certain ranges. These ranges are shown in EquationsEqs. (6) and (7). They differ because of the inclusion or disregard of the Arrhenius law, which include and exclude the Arrhenius factor, respectively. Optimal factors can be found within these range boundaries for every analysed ranges for every analyzed firn profile. To ensure thisthat this is the case, all simulations were performed multiple times testing using different ranges of the factors.

$$1.0\times10^{-9}\,\mathrm{K\,s^2\,kg^{-1}} \leq C_{\mathrm{v}_1,\mathrm{v}_2} \leq 2.5\times10^{-4}\,\mathrm{K\,s^2\,kg^{-1}} \tag{6}$$

$$2.5\times10^{-21}\,\mathrm{K\,s\,m^2\,kg^{-1}} \leq C_{\mathrm{v}_3,\mathrm{v}_4} \leq 5.0\times10^{-15}\,\mathrm{K\,s\,m^2\,kg^{-1}} \tag{7}$$

Figure 1 (b) shows the root mean square deviation (RMSD) b shows the RMSD plotted over the 250 tested values for the four different factors. The different variants are color coded variants are color-coded, and the best result is results are marked. The smallest value values of the deviation is shown within are shown in the figure. The corresponding density profiles are shown in Fig. 1 (a)a.

As can be seen in Fig. 1 (a) the The firn profile of ngt03C93.2 starts at a depth of aboutapproximately 1.3 m. This yields the problem of finding Therefore, an appropriate surface density , needed as boundary condition in the simulationboundary condition must be found. As firn density profiles differ greatly, especially near the surface, the derivation of an appropriate surface density is difficult. Following our approach we Although Alley (1987) simulated the density starting at a depth of 2 m below the surface, we included this domain in our simulation so that we could apply transient surface forcing to our model. To find suitable values of the surface density, we included this parameter in our optimization. For each of the four variants and 250 factors C_v, we tested 21 different values for values of the surface density between $\rho_0 = 250\,\mathrm{kg\,m^{-3}}$ and $\rho_0 = 450\,\mathrm{kg\,m^{-3}}$, using steps of $\Delta\rho_0 = 10\,\mathrm{kg\,m^{-3}}$. Afterwards the best result is chosen. This method proofed to work well throughout the study. Firn profiles which start The best result was chosen. We used the method of testing 21 surface density values for all the analyzed firn profiles. We included profiles including measurements of the density at small depths, providing near surface density data are well represented. Applying the method to all firn profiles no matter at which depth they begin, accounts for comparability of the results . Overall In this way, we established that the results are comparable. Profiles including near-surface density values are, however, well-represented. A total of $4\times250\times21 = 21\,000$ simulations were performed in case of for ice core ngt03C93.2 to find the optimal results shown in Fig. 1. The same procedure was applied to all 159 firn profiles analyzed in the study.

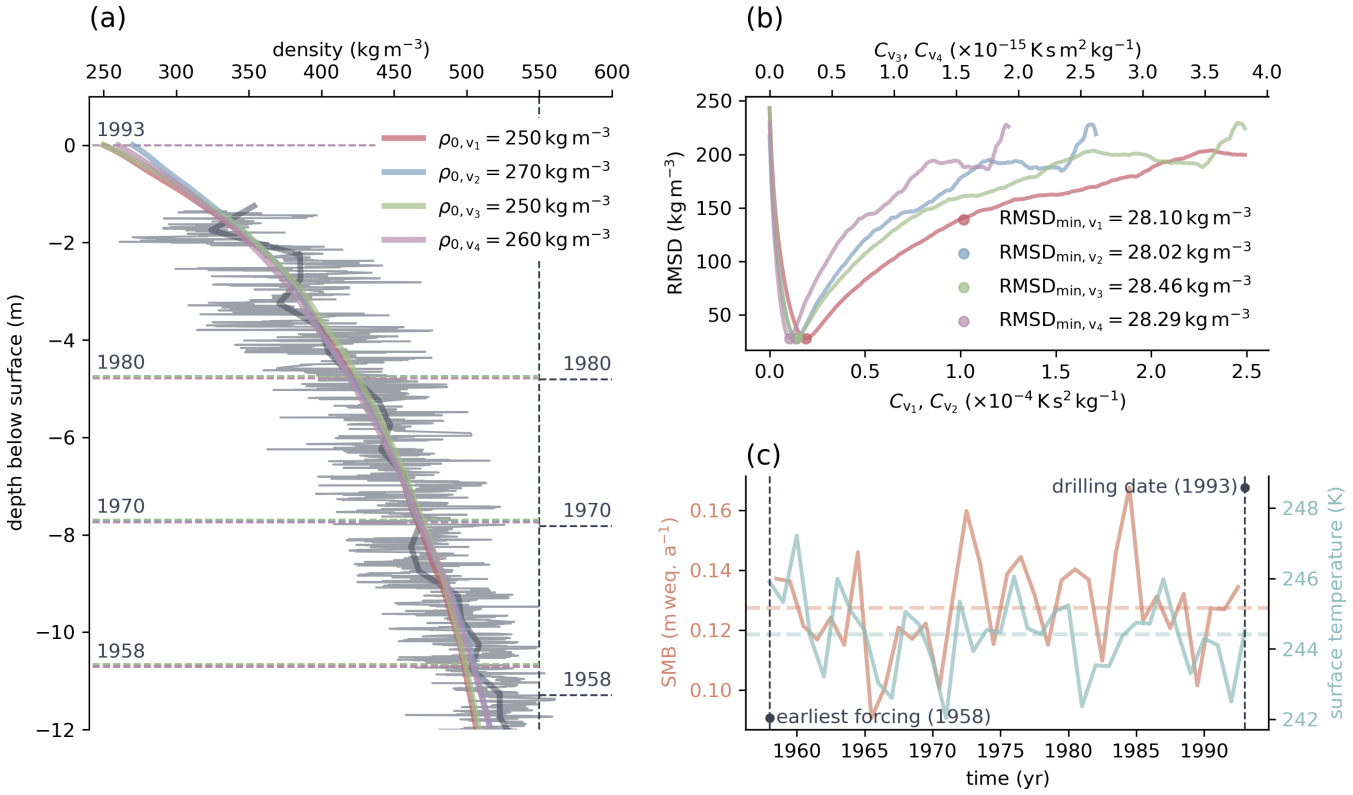

Figure 1. ~~Panel~~ (a) ~~of the figure shows the depth~~ Depth density profile of ice core ngt03C93.2 (Wilhelms, 2000) retrieved in Greenland ~~in~~ (gray~~colour~~) and ~~the~~ best corresponding model results obtained using four ~~different~~ variants of ~~the~~ constitutive law for grain boundary sliding ~~by~~ of Alley (1987) ~~in different~~ (various colors). ~~The strong~~ Dark gray line shows the mean density of the ice core calculated using a window of 0.5 m ~~,~~ starting at the surface. Dashed horizontal lines represent horizons of firn deposited in the indicated years, where 1958 ~~being~~ is the first year that forcing from RACMO2.3 (Van Wessem et al., 2014; Noël et al., 2015) is available. ~~Simulation results are drawn using colors as shown~~ Colored dashed horizontal lines show horizons obtained in the ~~legend~~simulations. Horizons plotted in gray ~~,~~ (to the right of the vertical dashed line~~,~~) represent the same surfaces as those determined by Miller and Schwager (2004) during analysis of the core. ~~Panel~~ (b) ~~shows the root mean square deviation~~ RMSD between measured and ~~modelled~~ modeled density plotted over the range of tested factor values. Note the different axes for different tested factors. ~~The~~ (c) Representative forcing ~~representative for~~ at the location of ice core ngt03C93.2~~and~~ , which was used in the simulation~~is shown in panel (c)~~. Horizontal dashed lines show the mean values of the surface mass balance and surface temperature ~~over~~ during the ~~course of the~~ simulation~~time~~.

3 Data

3.1 Firn ~~Profiles~~profiles

~~In order to test~~ To evaluate the description of grain boundary sliding given by Alley (1987), we ~~use~~ used 159 firn profiles~~of which 80~~ , 80 of which were retrieved in Greenland. The remaining 79 measurements were taken in Antarctica. The profiles are included in the ~~"Surface Mass Balance and Snow Depth on Sea Ice Working Group (SUMup)~~ SUMup snow density subdataset~~"~~ (Koenig and Montgomery, 2019). Individual references for all 159 firn profiles are listed in the supplementary material. The dataset does not ~~feature~~ include the four profiles used in the study ~~by~~ of Alley (1987), as the original data ~~of~~ for these firn cores are unpublished. To obtain firn profiles ~~relevant~~ suitable for this study from the dataset, we ~~filter it based on the following conditions~~filtered it according to the following criteria:

1. Profiles ~~have to~~ must consist of at least ~~ten~~ 10 data points.
2. The overall length of ~~the profiles has to exceed three meters~~each profile must exceed 3 m.
3. Profiles ~~have to~~ must start at a depth of less than ~~three meters below~~ 3 m below the surface.
4. The ~~starting~~ initial density of the profiles must not ~~to~~ exceed $\rho_c = 550\,\mathrm{kg\,m^{-3}}$.
5. The annual mean surface mass balance at the profile locations ~~has to be~~ must be strictly positive.
6. Forcing data ~~of~~ for at least five years ~~have to~~ must be available for the profile location.

~~While criteria 1. and 2. ensure general~~ Criteria 1 and 2 ensure the overall quality of the data, ~~conditions 3. and 4. guarantee~~ whereas criteria 3 and 4 ensure that the first stage of firn densification is ~~incorporated~~included. As the model ~~is not capable of handling melt~~ cannot handle melting, and the study focuses on dry firn densification, the surface mass balance should be positive, as stated in the fifth criterion. However, a positive mean annual surface mass balance does not ~~guarantee no melt~~ ensure that no melting occurs over the course of a year. ~~Based on the data available for this study a distinction between sites influenced by melt~~ It is not possible to distinguish between sites affected by melting and sites where no ~~melt occurs is not possible~~melting occurs using the data available for this study. The number of these sites~~however~~ , however, is expected to be small~~in comparison to the overall number of analysed firn profiles. Due to the method~~ . Because of the method used, their influence on the overall result is therefore small. ~~Forcing data comes~~ The forcing data come from the regional climate model RACMO2.3 (Van Wessem et al., 2014; Noël et al., 2015)~~. This~~ , which provides the surface mass balance. The model delivers data for ~~times from~~ the periods 1958 to 2016 and 1979 ~~until~~ to 2016 for Greenland and Antarctica, respectively (see also ~~Section~~Sect. 3.2). ~~Density~~ The density measurements used for model comparison should thus be retrieved during ~~this~~ these periods. We ~~chose to only use~~ used only datasets for which at least five years of forcing data ~~is~~ are available. Furthermore, a number of density profiles were manually excluded from the filtered data~~by hand. This incorporates profiles~~ . These profiles include those with very low spatial resolution, atypical profiles showing decreasing density with depth, and measurements with a surface density very close to the critical density of $\rho_c = 550\,\mathrm{kg\,m^{-3}}$. As explained in ~~Section~~Sect. 2.2 and illustrated in Fig. 1,

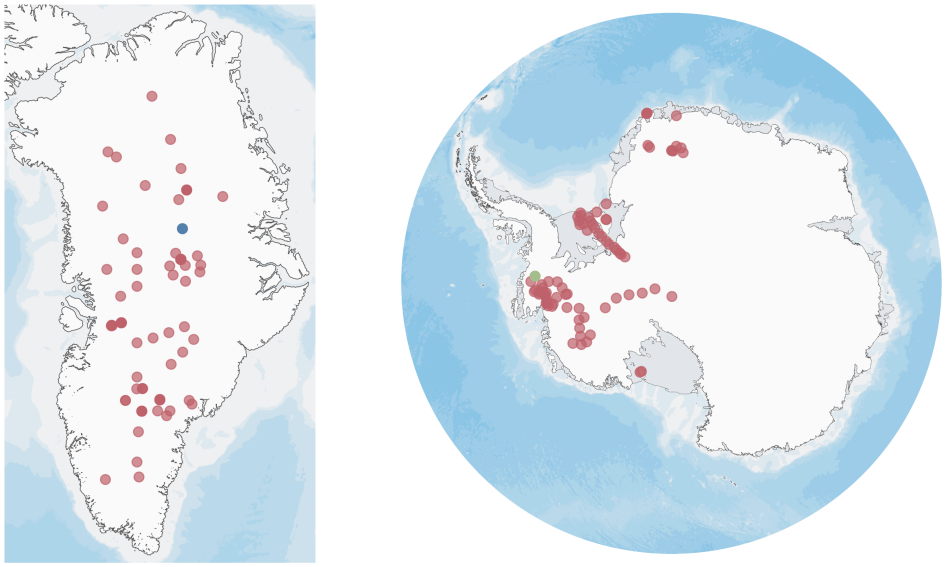

Figure 2. Locations of ~~the~~ firn profiles used for model ~~comparision~~comparison. ~~80~~ ~~Eighty~~ profiles were measured in Greenland, and 79 depth density datasets were retrieved in Antarctica. The blue marker shows the location of ice core ngt03C93.2 (Wilhelms, 2000, N 73.940°, E −37.630°). The green marker shows the location of site 3 of the iSTAR traverse, from which the firn core shown in ~~Figure~~Fig. ~~??~~ 3 was retrieved (Morris et al., 2017, N −74.565°, E −86.913°). Map data: Amante and Eakins (2009); Arndt et al. (2013), SCAR Antarctic Digital Database.

we ~~only use~~ used only a certain domain for the comparison ~~between~~ of the simulated and measured data. If this domain ~~turns out~~ was found to be less than 2.5 m long ~~in case of~~ for any of the tested variants of the constitutive equation, the firn profile in question ~~is neglected in the furtheranalysis~~was not analyzed further.

Figure 2 ~~illustrates~~ shows the locations from which the 159 density profiles were retrieved. The 80 measurements from Greenland are relatively uniformly distributed over the ice sheet. Coastal locations are not well covered ~~due~~ owing to the requirement of a strictly positive surface mass balance. In the Antarctic~~sites in east~~, sites in East Antarctica are underrepresented. However, a wide variety of environments is covered, including the ~~Filchner-Ronne~~ Filchner–Ronne Ice Shelf, the ~~west Antarctic coast~~West Antarctic coast, and Dronning Maud Land.

3.2 Boundary ~~Conditions~~ conditions and ~~Forcing~~forcing

To force the firn densification model, ~~surface values for~~ we need the surface values of density, temperature, accumulation rate, and grain radius at the locations of the 159 firn profiles~~are needed~~. Although Alley (1987) used constant forcing~~we follow~~, we followed the example of Arthern and Wingham (1998) and Goujon et al. (2003)~~performing~~, who performed transient simulations.

As measured firn density profiles represent past climate conditions, the choice of forcing data ~~is crucial for the presented method~~ in the proposed method is crucial. Uncertainties in the forcing will ~~reflect in~~ affect the simulation results and therefore ~~in~~ the comparison with the measured firn profiles. Neither the model formulation nor the ~~optimisation~~ optimization scheme can compensate for ~~that~~these effects. We ~~use~~ used data provided by the regional climate model RACMO2.3 (Van Wessem et al., 2014; Noël et al., 2015)~~5.~~. Details on RACMO2.3, including the limitations of the model and the resulting data products, were presented by Van Wessem et al. (2014); Noël et al. (2015); van Wessem et al. (2018). RACMO2.3 provides forcing data for the Greenland ice sheet covering ~~the period from~~ 1958 to 2016. ~~In case of Antarctica~~For Antarctica, the time period is shorter, ~~starting in~~ running from 1979 ~~and ending in~~ to 2016. Data for the mean annual skin temperature and surface mass balance ~~for~~ of the Greenland ice sheet are available at mean spatial resolutions of 11.3 km and 1.0 km~~respectively~~, respectively, for this study. ~~Mean spatial resolutions for Antarctica are 8.0 km and 28.5 km for~~ The mean spatial resolutions of the mean annual skin temperature and surface mass balance for Antarctica are 8.0 km and 28.5 km, respectively. ~~Spatial interpolation of the fields obtained from RACMO2.3 output leads to forcing data for the locations of the investigated firn profiles. It has to be mentioned that such an interpolation may introduce systematic errors.~~

The time period for the transient simulation runs, as described in ~~Section~~Sect. 2.2, is specified by the earliest data available from RACMO2.3 and the drilling date of the firn core under consideration. ~~In case of~~ For ice core ngt03C93.2 (Wilhelms, 2000), which was retrieved in central Greenland in 1993, the simulation time covers the period from 1958 to 1993 (see Fig. 1 ~~(c)~~c). Constant values of the surface temperature and surface mass balance for the preceding ~~spin up are~~ spin-up period were calculated as mean values over this time range.

~~Using~~ We present a second example ~~we want to illustrate how the~~ to illustrate the effect of the temporal resolution of the forcing ~~affects the optimisation~~ on the optimization results and why we ~~decided to use~~ used yearly averaged data provided by RACMO2.3. Figure ~~??~~ 3 shows the depth density profile of the firn core ~~retrived~~ retrieved at site 3 of the iSTAR Traverse in 2013 (Morris et al., 2017). The location of the site, at Pine Island Glacier in West Antarctica, is shown in Fig. 2. Instead of using forcing data from RACMO2.3, for this particular simulation we used ~~"~~ERA5-Land monthly averaged data from 1981 to present ~~"~~ (Muñoz Sabater, 2019; Hersbach et al., 2020), as ~~it is~~ they are freely available at monthly resolution. From ~~this datawe computed~~ these data, we computed the annual average data for a second simulation run. The forcing data at both resolutions ~~is~~ are shown in Fig. ~~?? (c). Panel (a) of the figure shows the best~~ 3c. Figure 3a shows the simulated firn profiles ~~identified using the optimisation approach in comparison with the~~ that best reproduce the measured density profile~~. On the left hand side results~~, which were identified using the optimization approach. The results obtained using the annually averaged forcing data are shown ~~, while the right hand side illustrates the results~~ on the left, whereas those obtained using monthly averaged data from ERA5 ~~. In case of the~~ are shown on the right. The data with higher resolution data reveal much more detail ~~is covered~~ within the simulated firn density profiles. However, the aim of this study is not primarily to reproduce the ~~analysed~~ analyzed measured firn profiles with the highest possible detail, but to evaluate the constitutive relation ~~by~~ of Alley (1987) using an ~~optimisation approach finding site specific~~ optimization approach that identifies site-specific optimal constitutive factors C_v (see ~~Section~~Sect. 2.2). ~~Panel (b) of Fig. ?? shows the root mean square deviation~~ Figure 3b shows the RMSD of the simulated profiles from the measured profile over the range of tested ~~optimisation~~ optimization factors. Dashed lines ~~belong to~~

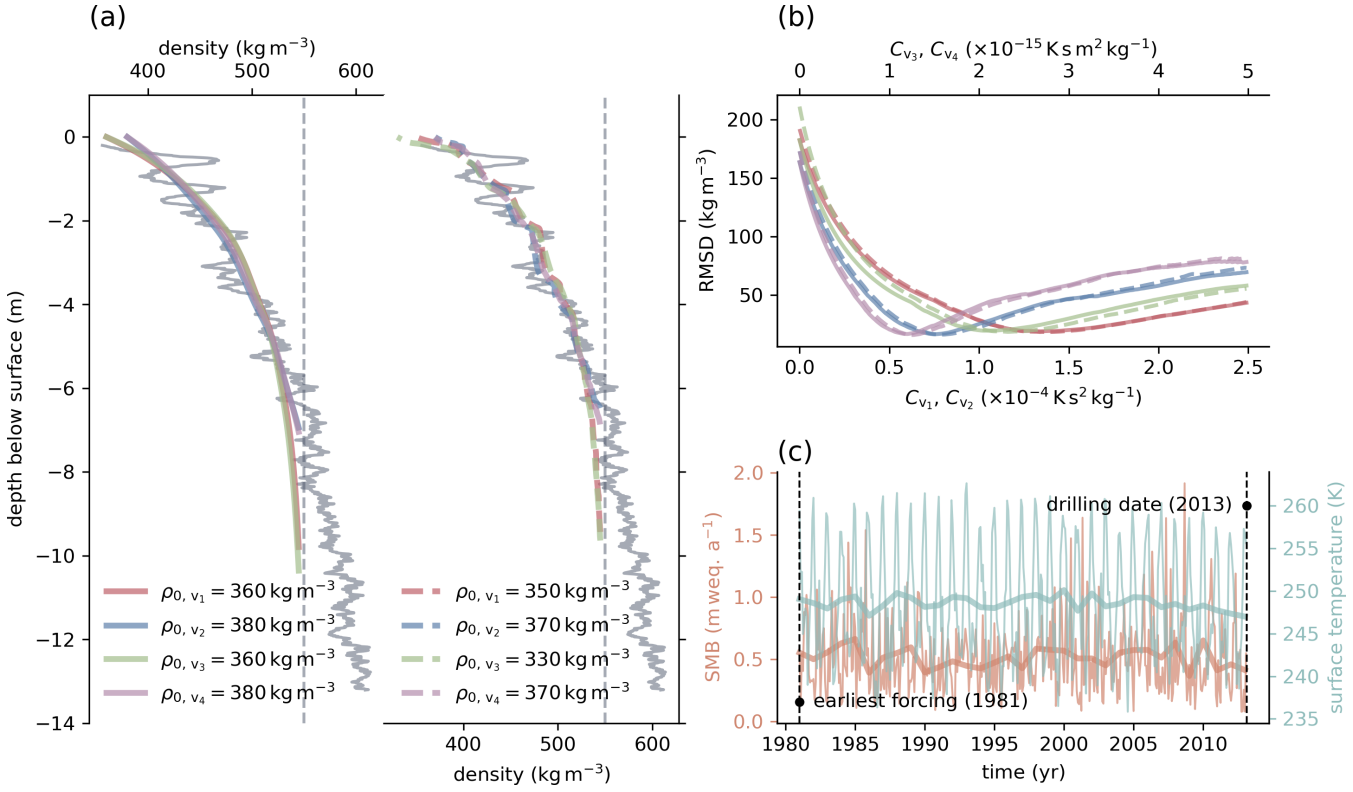

Figure 3. ~~Panel~~ (a) ~~of the figure shows the depth~~ Depth density profile (gray) of ~~the~~ firn core retrieved at site 3 of the iSTAR traverse (Morris et al., 2017)~~in gray colour~~. ~~Colour coded~~ Colored lines show the ~~optimised~~ optimal simulation results for ~~all~~ four tested variants of the constitutive relation~~are pictured~~. The simulated density profiles on the left ~~result from~~ were obtained using yearly averaged surface forcing~~while the profiles~~, whereas those on the right, plotted using dashed lines, ~~result from~~ were obtained using monthly averaged forcing. ~~In panel~~ (b) ~~the root mean square deviation (~~RMSD ~~)~~ between ~~the~~ best simulation result and ~~the~~ measured firn profile ~~is shown~~ over the range of tested ~~optimisation~~ optimization factors C_v. ~~Colours again~~ Colors indicate results for the different variants of the constitutive relation. Dashed lines ~~are used for~~ indicate results computed with monthly averaged forcing~~while~~, whereas solid lines indicate the use of yearly averaged surface forcing. ~~The forcing~~ (c) Forcing data from ~~"~~ERA5-Land monthly averaged data from 1981 to the present ~~"~~ (Muñoz Sabater, 2019; Hersbach et al., 2020)~~is shown in panel (c)~~, from the earliest available forcing in 1981 to the date the firn core was drilled in 2013. ~~Strong~~ Bold lines show ~~the~~ yearly averaged data computed from ~~the~~ monthly averaged data.

~~the~~ represent simulations performed using the ~~high resolution~~ high-resolution forcing data, ~~while solid lines are dedicated to~~ whereas solid lines represent the annual averaged data. The difference between the ~~optimisation~~ optimization results is small. We therefore ~~decided to use~~ used the annual averaged data provided by RACMO2.3 ~~, available~~ suitable for this study, as the data ~~covers~~cover a longer time period, especially for Greenland~~, a greater time period. This allows us to analyse~~ . As a result, we can analyze more firn profiles at greater detail. ~~In case of~~ For ice core ngt03C93.2 (Wilhelms, 2000), the horizon of the year 1981, the earliest forcing available in ERA5, lies at a depth of ~~about~~ approximately 5 m below ~~surface as can be seen~~ the surface, as shown in Fig. 1 ~~(a)~~a. The horizon of the earliest forcing available ~~by~~ from RACMO2.3, the year 1958, is located at a depth of ~~about~~ approximately 11 m below the surface. A much greater ~~part~~ portion of the simulated firn profile is therefore ~~influenced by the~~ affected by surface forcing. Furthermore, the use of yearly averaged data ~~produces~~ requires less overhead.

As ~~pointed out in Section 2.2we use~~ noted in Sect. 2.2, we used 21 surface density values in the range ~~of~~ $250\,\mathrm{kg\,m^{-3}} \leq \rho_0 \leq 450\,\mathrm{kg\,m^{-3}}$ for every tested firn profile. The value ~~leading to~~ that yielded the best result ~~is~~ was then used for further analysis. ~~Due to the~~ Owing to a lack of relevant data, ~~simplicity and better comparisonoptions~~ and for simplicity and ease of comparison, the grain radius at the surface ~~is~~ was assumed to be the same at all ~~location~~ locations and to be constant over time. We ~~chose to use~~ used a grain radius of $r_0 = 0.5\,\mathrm{mm}$ ~~based on the~~ on the basis of the measurements and empirical relation ~~by~~ of Linow et al. (2017) and the assumption of Arthern and Wingham (1998). As climatic conditions, and therefore the surface grain size~~differ at every investigated location this~~ , vary among the investigated locations, this choice is a simplification. ~~Due to the optimisation approach the influence of this parameter is of less significance~~ Owing to the use of the optimization approach, this parameter has a less significant effect, as it can be understood as a constant part of the grain radius, which is the same for every ~~analysed~~ analyzed firn profile.

Figure 4 illustrates the range and distribution of surface boundary conditions at the investigated sites. ~~In comparison~~ The locations in Greenland show a higher mean surface temperature and surface mass balance than ~~locations~~ those in Antarctica. The surface density is higher at ~~Antarctic location than~~ the Antarctic locations than at those in Greenland. ~~In general~~ Overall, a wide variety of typical climatic conditions for both ice sheets is covered.

3.3 Distribution and ~~Influence~~ effects of ~~Input Data~~input data

Ice core ngt03C93.2 ~~shown in~~ (Fig. 1 ~~(~~a) is an example of a ~~high resolution~~ high-resolution density measurement showing extensive ~~small scale~~ small-scale layering. Only a few of the 159 firn profiles are of such high quality and ~~cover such kind~~ include this type of layering. Although our ~~model approach works on a~~ proposed model works at high temporal and spatial resolution, it does not cover layering, as shown in Fig. 1 ~~(a).Simulation of small scale layering could easily be added to the model following the~~ a. The density profile retrieved at site 3 of the iSTAR traverse (Morris et al., 2017) (Fig. 3) illustrates that the model, if it is forced with data of higher temporal resolution, still does not cover the measured density variability. Small-scale layering of firn appears to be driven by a number of different processes (Hörhold et al., 2011). An extension of the model to cover such processes may be introduced in the future. We would prefer the approach of Freitag et al. (2013), ~~introducing a dependency of the activation energy Q_{BD} for the process of boundary diffusion (Equation (1)) on a proxy for impurities. Such data~~ who introduced the concept of impurity-controlled densification. Forcing data for this model are

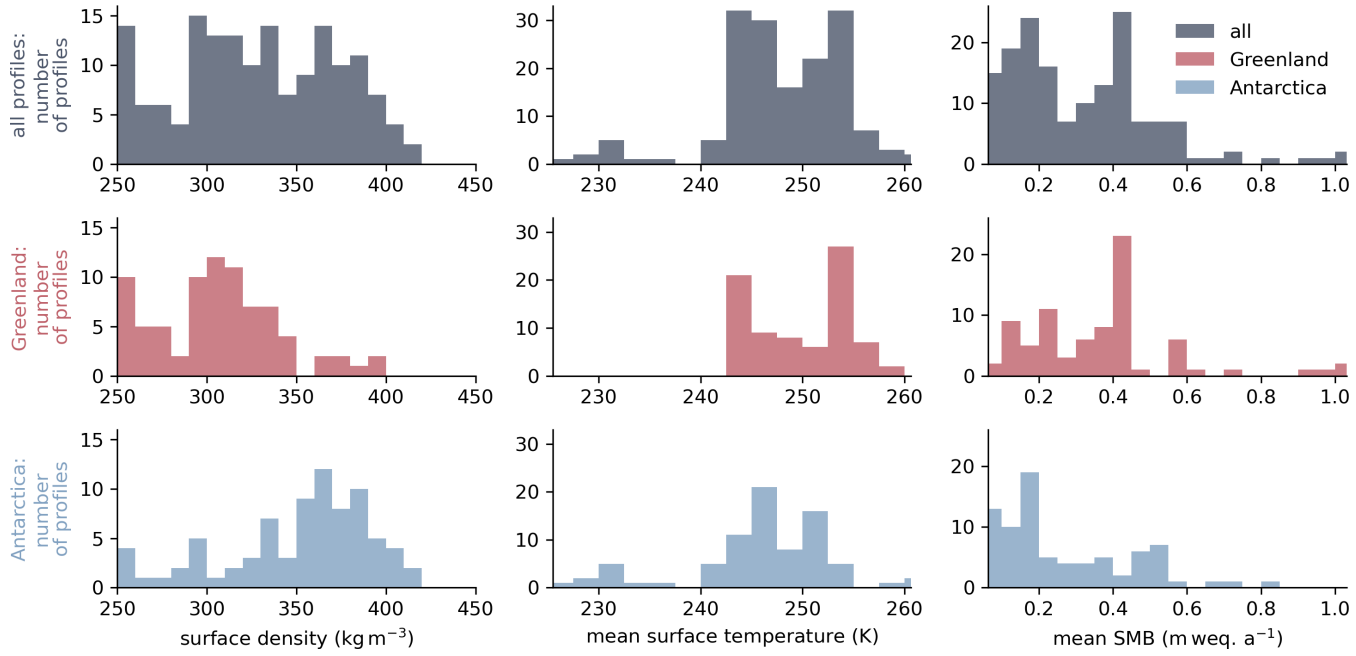

Figure 4. Distribution and comparison of ~~the~~ boundary conditions at the 159 firn profile sites. All values are averaged over the ~~specific~~ simulation time for ~~every~~ each location, beginning in ~~the year~~ 1958 ~~or~~ and 1979 for Greenland and Antarctica, respectively, and ending at the date of measurement (see ~~Section~~Sect. 3.2). The top row of plots ~~, in~~ (gray~~colour,~~) shows the boundary conditions at all locations, ~~while~~ whereas the middle and bottom ~~row~~rows, in red and blue, ~~exclusively represent~~ show only the locations in Greenland and Antarctica, respectively. Data for the surface temperature ~~in the middle,~~ (center) and surface mass balance ~~in the~~ (right column~~,~~) are provided ~~via~~ by RACMO2.3 (Van Wessem et al., 2014; Noël et al., 2015).

not globally available. ~~The activation energy can therefore be understood as a temporally averaged value, leading to a mean density. The use of the root mean square deviation for comparison of simulation results and measured density profiles assures the optimisation result is independent of layering. To illustrate this the running mean density of ice core ngt03C03.2 is shown~~ However, the model in its current form does reproduce the mean density well, as demonstrated in Fig. 1 ~~(a). Note that computing the running mean neglects information. Thus we compute the root mean square deviation on the basis of the original data.~~ a.

In this study~~we focus on the very first~~ , we focused on the initial stage of firn ~~densificaiton and the upper most meters~~ densification and the uppermost part of the firn column. We ~~limit~~ limited the model domain to a maximum depth of $-25\,\mathrm{m}$ below the surface. Furthermore~~we do~~ , we did not develop the density further after the critical density of $\rho_c = 550\,\mathrm{kg\,m^{-3}}$ ~~is~~ was reached. This choice raises the question ~~if~~ of whether the use of a Neumann boundary condition set to zero at the profile base to solve for the temperature ~~as described in Section A4~~ is justified for this particular model setup ~~.~~ (Sect. A4). The critical density of $\rho_c = 550\,\mathrm{kg\,m^{-3}}$ is ~~mostly~~ usually reached within the upper ~~ten meters~~ 10 m of the firn column. The temperature within this domain is ~~influenced by the~~ affected by surface conditions, which are covered by the forcing data. At

greater depths, the temperature corresponds to the mean annual surface temperature and changes very little ~~. The amount of high resolution temperature measurements in firn is sparse~~(e.g., Cuffey and Paterson, 2010, pp. 399 ff.). There have been few high-resolution temperature measurements of firn. Orsi et al. (2017) published a temperature profile of a $147\,\mathrm{m}$ length from borehole NEEM2009S1, which shows a temperature difference of little more than $1\,\mathrm{K}$ over the entire profile. ~~The study by~~ Vandecrux et al. (2021) ~~suggests the same . Such~~ obtained the same result. This small temperature change ~~, below the depth of~~ at depths greater than approximately $10\,\mathrm{m}$ below the surface has little effect on our model approach. To test the ~~sensitivity of the optimisation approachon the temperature we performed reruns of the simulations with the site specific~~ temperature dependence of the optimization approach, we performed the simulations again using the site-specific surface temperature forcing ~~increased and decreased by~~ plus or minus $1\,\mathrm{K}$. The effect on the optimal factors C_v ~~differs depending~~ depends on the variant of the constitutive relation, but ~~in general is~~ it is generally small. For example, the greatest difference between the optimal factors ~~resulting from~~ obtained using the correct and ~~the adjusted forcing in case of~~ adjusted forcing for ice core ngt03C93.2 (Wilhelms, 2000) ~~can be found when~~ were found using Variant 1. ~~It shows~~ This variant yields a value of $\Delta C_{\mathrm{v1,max}} = 0.02 \times 10^{-4}\,\mathrm{K\,s^2\,kg^{-1}}$, which corresponds to ~~two times~~ twice the sampling space of the factors $C_{\mathrm{v_1}}$ used in the ~~optimisation. In case of~~ optimization. Variant 4 ~~the results are even the same~~ yields the same results. Because of this small ~~influence in general, the greater influence~~ effect overall, the stronger effect of the surface temperature in the investigated domain~~and the restriction~~ , and the limitation of the comparison to the domain actually ~~influenced by the surface forcing~~affected by surface forcing, a Neumann boundary condition at the profile base ~~,~~ is justified despite the low depth~~, is justified~~.

4 Results

Figure 5 ~~illustrates~~ shows the distribution of the ~~root mean square deviation (RMSD)~~ RMSD calculated from the simulated firn profiles ~~matching~~ that best reproduce the measured profiles~~best~~. The four ~~different plots of the figure distinguish between the four different~~ plots in the figure represent the four variants of the constitutive equation for grain boundary sliding ~~(Equations~~[Eqs. (2) to (5)~~) ~~]~~, as described in ~~Section~~Sect. 2.2. Additionally~~the median value ~~, the median values of the data is~~ are shown. The ~~differences in the distribution~~ distributions of the deviation ~~are small with regard to the different tested variants~~ for the four variants show little difference. The median values differ in a small range. ~~Variant~~Variants 2 ~~shows the smallest value and Variant~~ and 3 ~~the greatest~~show the smallest and largest values, respectively. The use of the modification introduced by Bréant et al. (2017) ~~within~~ in the constitutive equation ~~results in 6.2 – 6.8 % better agreement between~~ improves the agreement between the simulated and measured firn profiles by $6.2–6.8\,\%$. To put the values in perspective, the deviation of the four ~~best fitting modelled~~ best-fitting modeled firn profiles from ice core ngt03C93.2 (Wilhelms, 2000) displayed in Fig. 1 is ~~about~~ approximately $28\,\mathrm{kg\,m^{-3}}$. That ~~means~~is, more than half of the ~~resulting~~ simulations show even better agreement with the corresponding firn density profiles than this one. An overview of the deviation ~~between~~ among all 159 measured firn profiles and the corresponding best simulation results can be found in the supplementary material.

The range of factors ~~resulting in the best fitting~~ contributing to the best-fitting firn profile is smaller for Variants 2 and 4 of the constitutive equation, which use the modification ~~by~~ of Bréant et al. (2017), compared to Variants 1 and 3, as shown in

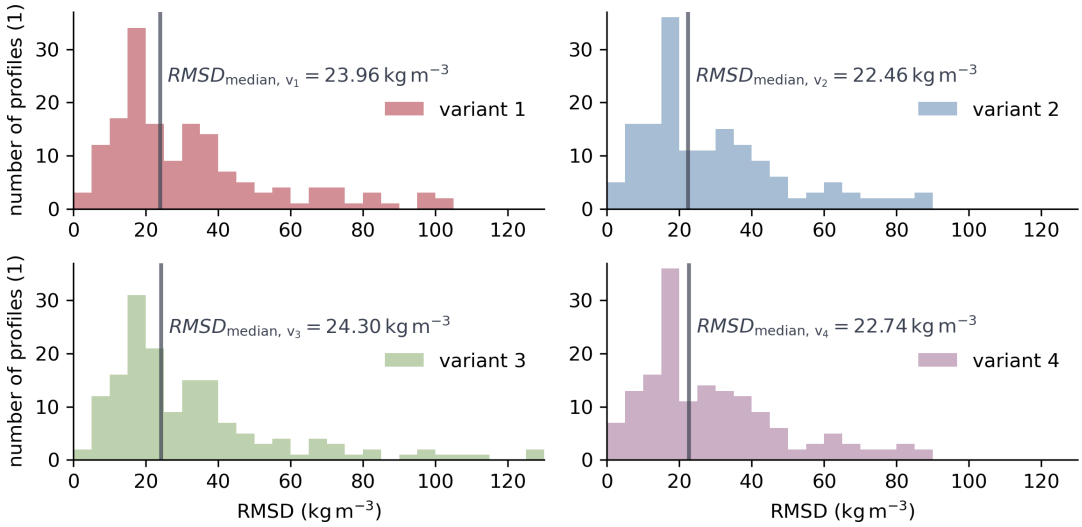

Figure 5. Distribution of ~~the~~ smallest ~~root mean square deviation (~~RMSD ~~)~~ for every ~~analysed~~ analyzed firn profile found using the ~~optimisation~~ optimization scheme outlined in ~~Section~~Sect. 2.2. The four plots show the results for the four tested variants of the constitutive equation. Vertical lines ~~illustrate~~ indicate the median ~~value~~ of the 159 values.

~~form of~~ the box plots in Fig. 6. In contrast to factors C_{v_1} and C_{v_2}, factors C_{v_3} and C_{v_4} incorporate the Arrhenius ~~law~~ factor from the original description of grain boundary sliding given by Alley (1987). Therefore~~a~~, direct comparison between the two groups of factors is not possible. The quartile coefficient of dispersion ~~, shown for~~ of the four variants, which is shown on the right side of Fig. 6, is a relative measure ~~for~~ of the scatter of the values. The coefficient reveals that the ~~resulting factors of~~ factors obtained for Variants 1 and 2 are defined in a ~~range narrower versus~~ narrower range than those of Variants 3 and 4. All four ~~resulting~~ sets of factors show ~~a slightly non uniform distribution, tending towards~~ slightly nonuniform distributions that tend toward smaller values.

~~To find a possible dependency of the resulting factors, leading to the best match between simulated and measured density profiles, Fig. 7 shows the~~

To check for possible mean surface temperature dependence of the 159 factors found by ~~the optimisation, plotted against~~ optimization, these values are plotted against each other in Fig. 7. The values of the mean surface temperature were calculated from the forcing data ~~specific~~ for each firn profile ~~'s~~ site. The left plot illustrates the results for Variants 1 and 2 in red and blue~~colour, while the right part of the figure shows the resulting~~ , whereas the right plot shows the factors for Variants 3 and 4 using green and purple markers, respectively. The legend ~~features~~ shows the Pearson correlation coefficient r_{Pearson}, a measure ~~for~~ of the linear correlation of the two variables, and the distance correlation $dCor$ (Székely et al., 2007). The distance correlation was designed by Székely et al. (2007) to overcome problems ~~of~~ with the Pearson correlation coefficient. It describes the correlation of two vectors ~~while not being restricted to linear dependency~~and is not limited to linear dependence. It is defined ~~in the range~~ between zero and one, where zero indicates the independence of the variables.

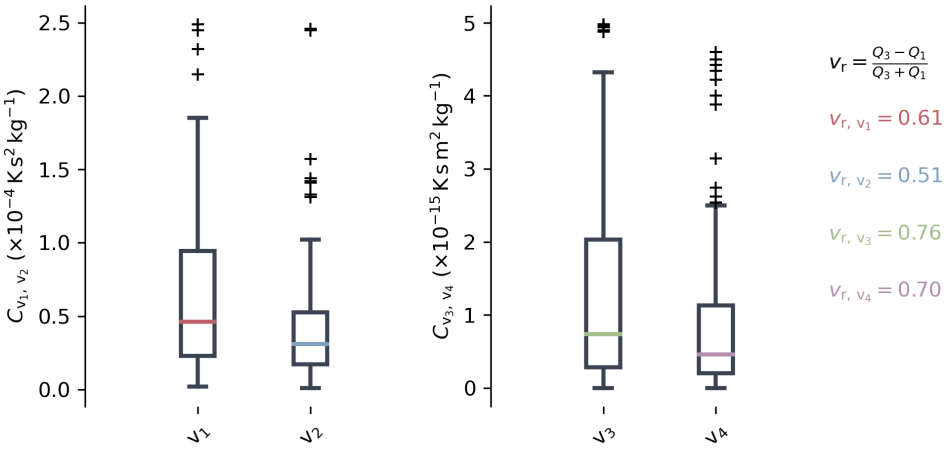

Figure 6. Box plots showing the distribution of the best factors, $C_{\mathrm{v}1}$ to $C_{\mathrm{v}4}$, for the four variants of the constitutive equation describing grain boundary sliding ~~(see Equations~~[Eqs. (2) to (5)~~),~~] derived using the ~~optimisation~~ optimization scheme described in ~~Section~~Sect. 2.2. ~~On the right side the quartile~~ Quartile coefficient of dispersion v_{r} of each variant is shown ~~for~~ on the ~~variants~~ right in the corresponding ~~colors~~color. The quartile coefficient of dispersion ~~is~~ was calculated using the first (Q_1) and third (Q_3) quartile values of the data sets~~as~~, which are shown in black ~~colour~~ and ~~represents~~ represent a robust relative measure of dispersion.

The correlation ~~of~~ between the resulting factors ~~with~~ and the mean surface temperature is higher compared to the correlation with other properties. This statement is especially true for factors $C_{\mathrm{v}3}$ and $C_{\mathrm{v}4}$ of Variants 3 and ~~4.~~ 4, respectively. However, the Pearson correlation coefficient ~~only indicates the~~ indicates only a linear correlation. The scatter of factors $C_{\mathrm{v}3}$ and $C_{\mathrm{v}4}$ with respect to ~~the~~ mean surface temperature might resemble a ~~higher order function~~higher-order function, as indicated by the higher values of the distance correlation.

~~Values~~ The values of the Pearson correlation coefficient and distance correlation shown in Fig. 8~~are higher than in Fig. 7. The figure shows the resulting factors in the same manner as Fig. 7 but~~ , which shows the factors with respect to ~~the~~ mean surface mass balance~~. Just as~~ , are higher than those in Fig. 7.

Like the mean surface temperature, the mean surface mass balance ~~is~~ was calculated from the forcing data used during the simulations. The correlation coefficients for the results ~~of~~ obtained using Variants 3 and 4 exceed ~~the ones for the~~ those for the results obtained using the variants of the constitutive equation incorporating the Arrhenius ~~law explicitly. The~~ factor explicitly. Variant 3 shows the best indication of a relationship between surface mass balance and the factor yielding the ~~factor resulting in the~~ density profile ~~best matching~~ that best reproduces the corresponding field measurement~~and the surface mass balance can be seen for Variant 3.~~ .

~~A striking feature within~~ In Fig. 8~~can be found~~ , a striking feature appears around a mean surface mass balance of $0.4\,\mathrm{m\,weq.\,a^{-1}}$. ~~Values~~ The values of the factors ~~resulting in the best match between simulation results and measured density~~ yielding the simulated density profiles that best reproduce the measured profiles show a wide range for all four variants of the constitutive relation. ~~The corresponding~~ These profiles are part of a study ~~by which took place~~ in western Greenland by Harper et al. (2012).

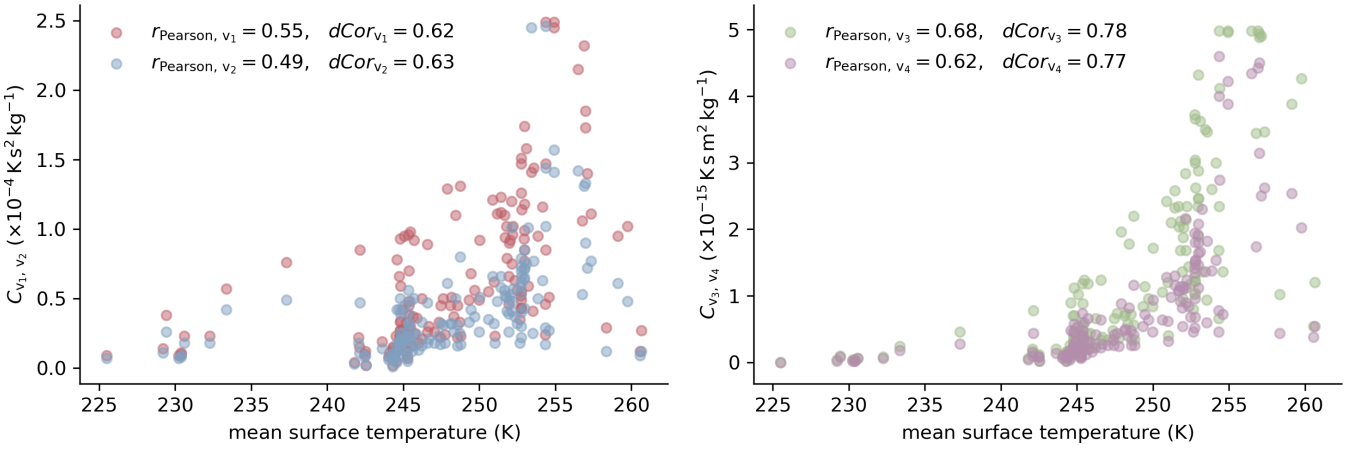

Figure 7. Best factors for every investigated firn profile ~~,~~ determined using the ~~optimisation~~ optimization scheme ~~,~~ and plotted against ~~the~~ mean surface temperature during ~~the~~ forcing period (see ~~Section~~Sect. 4). ~~On the left side of the figure the~~ Left: results for Variants 1 and 2 of the constitutive equation ~~are shown~~ in blue and red~~colour respectively~~, ~~while the right plot illustrates the~~ respectively. Right: results ~~of~~ for Variants 3 and 4 in green and purple~~colours~~, respectively. The Pearson correlation coefficient r_{Pearson}, ~~representing~~ which represents the linear correlation between factors C_{v_1} to C_{v_4} and the mean surface temperature, as well as the distance correlation $dCor$, are given ~~within~~ in the legend.

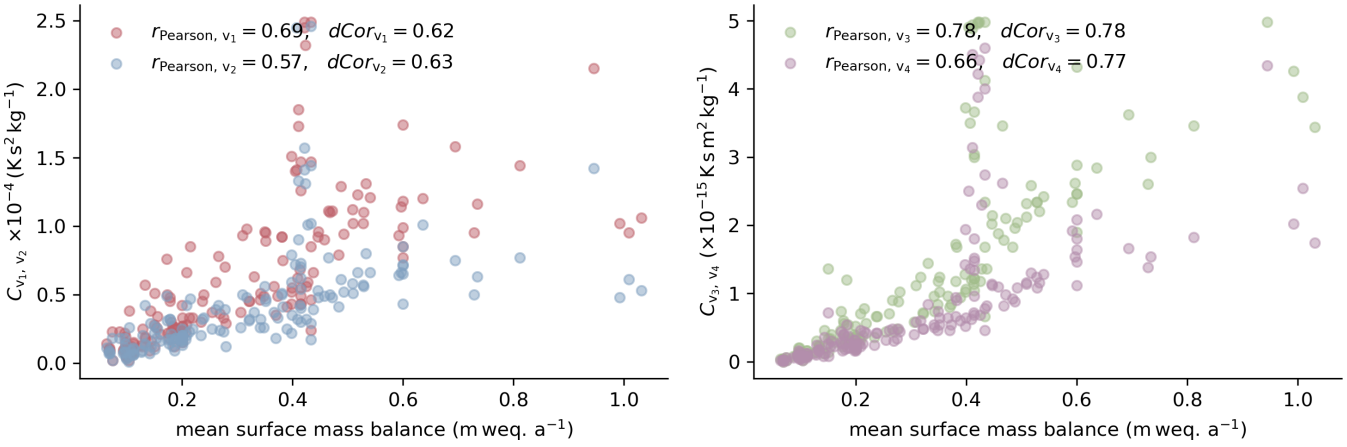

Figure 8. ~~Resulting factors of the optimisation over the~~ Factors obtained by optimization versus mean surface mass balance, calculated for ~~everyone of the~~ 159 firn profiles from ~~its~~ the forcing. ~~The left hand side plot shows best fitting~~ Left: best-fitting values for Variants 1 and 2 (factors C_{v_1} and C_{v_2}, respectively). ~~The plot on the right shows the corresponding~~ Right: best-fitting values for Variants 3 and 4 ~~or~~ (factors C_{v_3} and C_{v_4}, respectively). ~~The linear~~ Linear correlation between the factors and mean surface mass balance is ~~illustrated~~ indicated by the Pearson correlation coefficient r_{Pearson}, and the general correlation is indicated by the distance correlation $dCor$.

The study region is relatively small, which explains the similar climatic conditions. Although the mean annual surface mass balance is positive, melting occurs throughout the year ~~influencing~~ and affects the firn density.

5 Discussion

Using the four variants of the constitutive relation ~~by~~ of Alley (1987) ~~(Equations~~[Eqs. (2) to (5)~~) we were able to generate density profiles matching~~], we generated density profiles that were in good agreement with most of the 159 density measurements~~well~~. Uncertainties may ~~arise~~ result from the forcing, ~~the limited knowledge on~~ limited knowledge of the initial grain radius, and the poor constraint on the density at the surface. As measured firn densities represent past climate conditions, ~~deviant forcing would always result~~ unrealistic forcing always results in a mismatch between the simulated and measured firn properties, independent of the ~~optimisation~~ optimization approach and physical model. However, when the proposed optimization scheme was used, the differences between the ~~presented optimisation scheme leads to distinct minima of the deviation between~~ simulated and measured density profiles ~~, indicating~~ show distinct minima, indicating that the forcing represents the climatic history of the firn profiles, in principle.

The ~~optimisation scheme results in site specific values for~~ optimization scheme produces site-specific values of the factors C_{v_1} to C_{v_4}. As the ~~optimisation is specific for the analysed site and variant of the constitutive relation~~ optimization process is unique to each analyzed site and constitutive relation variant, the four simulated density profiles for ~~one specific~~ each site are very similar, as ~~is~~ illustrated in Fig. 5. This feature allows us to compare the factors ~~resulting from~~ obtained using the four variants. The differences between the factors do not ~~primarily arise~~ arise primarily from differences in the simulated density profiles, but reflect the differences in the variants~~, leading to~~ ; consequently, the results are almost the same~~result~~.

However, ~~due to the principle of the optimisation schemepossible errors included~~ owing to the nature of the optimization scheme, possible errors in the forcing data or other parameters ~~like~~ such as the activation energy used ~~for the computation of the~~ to calculate the grain radius (see ~~Equation~~Eq. A11) are also included in the ~~site specific~~ site-specific optimal factors C_{v_1} to C_{v_4}. If~~for example~~ , for example, the surface temperature forcing at a site ~~is constantly off by five degree Kelvin over the simulationtime, this~~ consistently deviates by 5 K during the simulation, this error can be compensated by ~~a corresponding adjustment of the specific optimisation~~ adjusting the specific optimization factor C_{v} (see ~~also Section~~Sect. 3.3). However, the ~~great amount of analysed~~ large number of analyzed firn profiles compensates for such random ~~error. Systematic error included~~ errors. Systematic errors in the forcing data ~~can not~~ van Wessem et al. (2018) cannot be identified. Therefore, ~~improvements~~ improving the temporal resolution of the forcing ~~with respect to resolution in time and covering of longer periods , could lead to~~ and covering longer periods could result in better and more detailed simulation results~~in future as is~~ , as shown in Fig. ~~??~~3.

~~It should be mentioned again~~This study analyzed only dry firn densification. The current model cannot handle melting. We accommodate this feature by setting the annual mean surface mass balance at the investigated sites to be strictly positive (Sect. 3.1). However, this limitation means that we cannot ensure that no melting occurs over the course of a year. The results shown in Fig. 8 illustrate how this limitation affects the optimization results. The limitation is problematic, especially in recent years, when melting occurred over almost the entire Greenland Ice Sheet (e.g., Nghiem et al., 2012). The simulation of

meltwater percolation through the firn and its interaction with firn densification is important, especially in the upper part of the firn body (e.g., Vandecrux et al., 2020). The proposed method could be improved by the application of this model approach in future investigations. However, we identified some correlations between the optimization results and the surface mass balance.

Note, again, that we have not investigated whether grain boundary sliding is indeed the ~~dominating~~ dominant process during the first stage of firn densification. We assess whether a process with a functional dependence on density, firn overburden stress, temperature, and grain radius ~~, is representing~~ represents the observed density profiles well. Any other deformation process with the same functional dependence would be equally well suited. Nevertheless, by maintaining the general structure of the constitutive relation ~~by~~ of Alley (1987), we conclude that this description of grain boundary sliding is a good basis for a physically based model describing firn densification up to the critical density~~of~~ , $\rho_c = 550\,\mathrm{kg\,m^{-3}}$.

Comparing the results for Variants 1 and 2, as well as those for Variants 3 and 4, we ~~find that the~~ found that an adjustment of $\left(1 - \frac{5}{3}\,\rho/\rho_{\mathrm{ice}}\right)$ to $\left(1 + \frac{0.5}{6} - \frac{5}{3}\,\rho/\rho_{\mathrm{ice}}\right)$ ~~is leading to better matches with~~ results in better reproduction of the measured density profiles. ~~With regard to~~ This result must be reviewed carefully in terms of the study design and the background of a ~~physics based~~ physics-based model describing firn densification~~, this result has to be reviewed carefully~~. As Alley (1987) ~~points~~ pointed out, grain boundary sliding might be the dominant process driving ~~the~~ firn densification at low densities, but it is presumably not the only one. The constitutive law ~~by~~ of Alley (1987) is designed ~~in a way~~ such that the densification due to grain boundary sliding becomes zero at ~~the~~ a density of $\rho_c = 550\,\mathrm{kg\,m^{-3}}$, ~~motivated by~~ owing to the densest packing of spheres obtained at that density and increasing accommodation incompatibilities. The modification ~~by~~ of Bréant et al. (2017) changes this ~~behaviour in the way that the process~~ behavior such that grain boundary sliding vanishes at a density of ~~about~~ approximately $\rho_c^* = 596\,\mathrm{kg\,m^{-3}}$, which could have advantages for the transition into the next stage of firn densification. We suggest ~~a simultaneous decline of~~ that a simultaneous decrease in grain boundary sliding and increase ~~of~~ in one or more other processes would provide a good ~~characterisation. Namely~~ characterization. Specifically, dislocation creep drives ~~the~~ densification at higher density (Maeno and Ebinuma, 1983) ~~due to~~ because of increasing stresses. ~~An~~ The onset of dislocation creep at densities ~~lower than~~ below $\rho_c = 550\,\mathrm{kg\,m^{-3}}$ ~~affecting not necessarily~~ would not necessarily affect the entire bulk firn matrix, but increasing volume fractions of the porous matrix~~should be investigated further in future~~.

Variants 1 and 2 of the constitutive relation ~~by~~ of Alley (1987) incorporate the Arrhenius ~~equation~~ factor for boundary diffusion, D_{BD}, from the description of the bond viscosity given by Raj and Ashby (1971). ~~For~~ In the formulation of Variants 3 and 4, we neglected the Arrhenius ~~equation. As can be seen~~ factor. As shown in Fig. 5, the difference in the resulting ~~root mean square deviation is small , whether the Arrhenius equation~~ RMSD is small regardless of whether D_{BD} is considered~~or not. This is consistent as we determine~~ . This result is reasonable, as we determined individual factors C_{v} for ~~every~~ each site. The similarity of the results allows us to compare the factors C_{v_1} and C_{v_2}, which were determined ~~including the Arrhenius equation~~using the Arrhenius factor D_{BD}, to factors C_{v_3} and C_{v_4}, ~~resulting from~~ which were obtained using the variants of the constitutive relation without the Arrhenius ~~equation. As the Arrhenius equation~~ factor. As D_{BD} is a function of temperature, it is reasonable to ~~take a look at the dependency~~ examine the dependence of the factors on the mean surface temperature~~as~~ , which is shown in Fig. 7.

The ~~determined~~ factors C_{v_3} and C_{v_4}, ~~resulting from variants without the Arrhenius equation for boundary diffusion~~ which were determined using the variants without D_{BD}, show a stronger ~~dependency~~ dependence on the mean surface temperature than the factors C_{v_1} and C_{v_2}. ~~At the same time,~~ In addition, the factors C_{v_1} and C_{v_2} show less dispersion than ~~factors~~ C_{v3} and C_{v_4}, as ~~is~~ shown in Fig. 6. The inclusion of ~~the Arrhenius equation~~ D_{BD} in the constitutive relation ~~leads to better~~ improves the determination of these factors. It is therefore a meaningful description within the constitutive relation. Although the inclusion of the Arrhenius ~~equation results in better determination of factors~~ factor improves the determination of C_{v_1} and C_{v_2}, we still see ~~a dependency~~ some dependence on the mean surface temperature~~to some degree~~. A better determination of the parameters of the Arrhenius ~~equation may result in resolving this dependency~~factor may resolve this dependence. If this is not the case~~another dependency~~ , another dependence on the temperature may be introduced to improve the constitutive relation for grain boundary sliding.

We interpret the ~~dependency on the~~ dependence on surface mass balance ~~such,~~ as indicating that the load ~~situation~~ is currently not represented well. The stress is represented by a second~~order~~ -order tensor. A firn column represented ~~in a one dimensional modelling~~ by a one-dimensional modeling approach would be surrounded by ~~neighbouring~~ neighboring firn columns, ~~a lateral confinement restricting deformation in~~ resulting in lateral confinement that limits deformation in the horizontal direction. The horizontal components of the stress tensor are not zero. As firn is a compressible material, the determination of these horizontal stress components is not trivial. The frequently used term "overburden pressure" is misleading, as the mechanical pressure is defined as the spherical part of the Cauchy stress tensor (e.g., Haupt, 2002, p. 301) and is not~~in general~~ , in general, identical to the normal stress in the vertical direction. With increasing depth, the magnitude of the horizontal stress components and their ~~influence would rise. Modelling approaches including considerations of~~ effects would increase. Modeling approaches that consider the full stress tensor ~~can be found in~~ were reported by Greve and Blatter (2009), Salamantin et al. (2009), and Meyer and Hewitt (2017). It might be ~~worthwhile to use~~ worth using the constitutive relation for grain boundary sliding ~~by~~ of Alley (1987) in such a ~~modelling~~ modeling context. This ~~must~~ approach will not necessarily result in a full ~~three dimensional model~~three-dimensional model, as the problem can be formulated ~~axially symmetrical. This would require an~~ assuming axial symmetry, which would require adjustment of the constitutive relation. A more extensive interpretation of the factors ~~obtained in the best matches~~ that yielded the best agreement is therefore challenging. The determination of a single factor C_v for one or all of the variants is not useful. It would not result in better simulation results compared to other published firn densification models. The ~~site specific~~ site-specific values of the factors ~~,~~ determined using the presented ~~optimisation approach ,~~ optimization approach simply show the differences in the variants of the constitutive relation.

6 Conclusions

Using variants of the constitutive relation for grain boundary sliding ~~by~~ of Alley (1987) and ~~a efficient optimisation~~ an efficient optimization scheme, we ~~were able to reproduce~~ reproduced 159 firn density profiles reasonably well. Thus~~we conclude,~~ , we conclude that the description of grain boundary sliding ~~as~~ introduced by Alley (1987) is appropriate for the simulation of firn densification at low density.

The modification of the constitutive relation ~~by~~ of Bréant et al. (2017) ~~leads to~~ results in slightly better simulation results when only the first stage of firn densification is considered~~solely. Further considerations~~ . Further factors, including the transition from the first to the second stage~~had to answer the question~~ , must be considered to answer questions regarding in which domain and to ~~which~~ what extent different processes ~~driving the densification~~apply~~drive~~ firn densification.

In our ~~optimisation approach~~optimization approach, we use a single factor representing various model parameters and search for the factor value ~~leading to the best match between~~ resulting in the best agreement between the simulated and measured firn profiles. ~~In this way the site specific~~ Consequently, the site-specific simulation results are independent of the possibly deficient ~~, now collectively considered, model parameters~~model parameters, which are considered collectively. It is not possible to derive a distinct value for the factor representing the climatic conditions at all locations of the investigated firn profiles. ~~The use of a global factor would lead to worse simulation results compared to existing firn density models. Rather we find a linear dependency~~ We found a linear dependence of the factors on the site-specific surface mass balance ~~specific to the location~~(Fig. 8). By contrast, we did not find a clear linear dependence on temperature (Fig. 7), but the results show that a site-specific parameter is required.

As the amount of surface accumulation affects the load ~~situation~~conditions, we assume it is not represented well in the model. Unlike other firn densification models, the physical ~~approach~~ simulation of grain boundary sliding ~~depends not~~ does not depend directly on the surface mass balance, but depends on the actual stress. Further interpretation of the ~~resulting~~ obtained factors is difficult using the presented simulation setup. The description of grain boundary sliding given by Alley (1987) could ~~benefit from a higher dimensional approach including~~ be improved by using a higher-dimensional approach including the horizontal components of the stress tensor. ~~Modelling approaches of such kind include~~ Modeling approaches of this kind include those of Greve and Blatter (2009), Salamantin et al. (2009), and Meyer and Hewitt (2017).

We ~~want to emphasise, that any kind optimisation approaches are only possible due to~~ would like to emphasize that optimization of any type is possible only because of the enormous efforts of the SUMup team (Koenig and Montgomery, 2019), ~~that~~ which has made a vast amount of firn core data available. ~~This is~~ These data are strategically crucial for ~~firn densification modelling advances, which adds to~~ advances in firn densification modeling, reinforcing the recommendations of FirnMICE (Lundin et al., 2017) for enhanced efforts ~~for~~ toward physically based models.

Code availability. The code used to simulate firn profiles will become available via github.com and gitlab.com when this manuscript is published.

Appendix A: Model description

A1 Numerical ~~Treatment~~ treatment of ~~Densification~~densification

All model equations are solved on an adapting ~~one dimensional grid , updated in~~ one-dimensional grid that is updated at every time step. The approach ~~follows the concept of~~ is based on an updated Lagrangian description~~with~~ , where the update velocity

of the grid ~~being~~ is the material flow velocity. This results in ~~material fixed~~ material-fixed coordinates. The ~~Lagrangian like description allows for a~~ Lagrangian-like description affords very high spatial and temporal resolution in the simulations. It can be shown that by integrating the local Eulerian form of the mass balance in one dimension over a material control volume with moving boundaries $z_1(t)$ and $z_2(t)$~~leads to~~ , we obtain (Ferziger and Perić, 2002, p. 374) ~~:~~

$$\frac{d}{dt}\int_{z_1(t)}^{z_2(t)} \rho\, dz + \int_{z_1(t)}^{z_2(t)} \frac{\partial}{\partial z}\left(\rho\left(v - v_b\right)\right) dz = 0\,. \tag{A1}$$

Here ρ ~~describes~~ represents the density, z is the vertical coordinate, t ~~the time~~ is the time, and v is the material flow velocity, whereas v_b represents the grid velocity or the velocity of the integration boundary. When the grid velocity equals the material flow velocity ($v_b = v$), the second ~~part of Equation~~term of Eq. (A1), ~~describing~~ which describes the advection, vanishes. The resulting equation is equal to the Lagrangian form of the mass balance (Ferziger and Perić, 2002, p. 374). On a ~~one dimensional grid , built up by~~ one-dimensional grid consisting of a number of grid points, as illustrated in Fig. A1, we ~~define~~ denote the grid point velocity ~~to be~~as v_b~~and to equal~~ , which is equal to the flow velocity $v_b \equiv v$. The ~~location~~ locations of all grid points ~~is updated in every~~ are updated at each time step by integrating the grid point velocity v_b using a forward Euler scheme. ~~In this way advection is entirely represented~~ Thus, advection is represented entirely by the adapting grid.

The grid point velocity v_b is calculated using the constitutive equation ~~of~~ for grain boundary sliding, as described in ~~Section 2.1~~Sect. 2.1, and the definition of the strain rate in one dimension. The description of grain boundary sliding provides the strain rate in the vertical direction along the grid, $\dot{\varepsilon}_{zz}$, as a function of ~~the~~ vertical stress σ_{zz}, density ρ, temperature T, and grain radius r

$$\dot{\varepsilon}_{zz} = f\left(\sigma_{zz}, \rho, T, r\right) = \frac{\partial v}{\partial z} = \frac{\partial v_b}{\partial z}\,. \tag{A2}$$

The strain rate of a material line element can be defined as the spatial derivative of the velocity, as shown in ~~Equation~~Eq. (A2) (Haupt, 2002, pp. 32–38). On a ~~one dimensional grid, defined by~~ one-dimensional grid, which is defined as a number of grid points, the space between ~~neighbouring~~ neighboring grid points can be considered as a material line element (see Fig. A1). Therefore, the grid point velocity v_b ~~can easily be~~ is easily computed by integrating the strain rate $\dot{\varepsilon}_{zz}$ in the vertical direction along the length of the grid cell:

$$v_b = \int_{z_1}^{z_2} \dot{\varepsilon}_{zz}\, dz\,. \tag{A3}$$

~~For the implementation of Equation~~To implement Eq. (A3), an integration constant determined by a suitable boundary condition is needed. It is reasonable to apply a Dirichlet boundary condition ~~, forcing~~ that forces the grid point velocity v_b to be zero ~~,~~at either the top or the base of the computational domain ~~, representing~~ to represent a fixed reference point at the top or the base of the ~~modelled~~ modeled firn profile, respectively. All other points defining the adapting grid are moving with respect to this anchor point. In ~~case of the present studywe decided to place~~ this study, we placed the anchor point at the base of the simulated firn profiles (z_0 in Fig. A1). ~~Depth coordinates of~~ The depth coordinates of the profiles shown in ~~following figures~~ the figures below were adjusted for better readability.

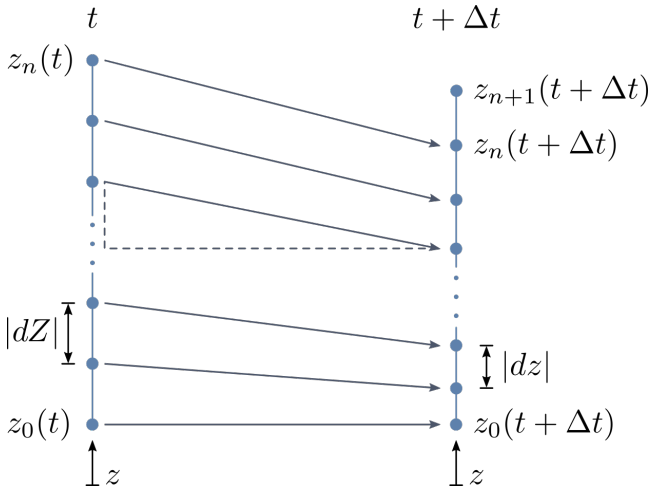

Figure A1. Principle of ~~the~~ grid evolution. ~~On the left side a~~ Left: grid at time t ~~is shown~~. ~~The~~ Right: updated grid at time $t + \Delta t$ ~~is illustrated on the right hand side of the figure~~. The grid points move ~~with~~ at the grid point velocity v_b, which ~~equals~~ is equal to the material flow velocity v. At time $t + \Delta t$, an additional grid point z_{n+1} representing accumulation is added. Distances between ~~neighbouring~~ neighboring grid points can be understood as material line elements $|dZ|$ and $|dz|$ in the reference and in the current configuration, respectively.

~~For the representation of~~ To represent accumulation at the top of a simulated firn profile, an inflow boundary condition ~~has to~~ must be implemented. To ~~achieve this , in every~~ this end, at each time step an additional grid point is added at the top of the grid. Its coordinate within the grid $z_{n+1}(t + \Delta t)$ is calculated ~~by~~ as

$$z_{n+1}(t + \Delta t) = z_n(t + \Delta t) + \Delta t\, a_0(t)\, \frac{\rho_{\text{water}}}{\rho_0}\,, \tag{A4}$$

~~with~~ where a_0 is the accumulation rate given ~~in~~ as the $m\,s^{-1}$ water equivalent, Δt is the length of the time step, ρ_{water} is the density of water, and ρ_0 is the density of the deposited snow. The position of a new grid point ($z_{n+1}(t + \Delta t)$ in Fig. A1) is the position of the firn surface at the last time step z_n plus the thickness of the firn layer deposited during the last time step. This thickness is defined by the time ~~time~~ step Δt and the ~~time dependent~~ time-dependent accumulation rate $a_0(t)$. ~~As we~~ We use an accumulation rate given in the unit of meter water equivalent per second, ~~it has to~~ which must be converted to the unit of meter firn equivalent taking the ~~site specific~~ site-specific surface firn density ρ_0 and water density ρ_{water} into account.

~~This processresults in a growing~~ In this process, the number of grid points ~~. Therefore~~ increases. Therefore, grid points are removed from the ~~extending~~ model domain at its base when a maximum number is reached.

A2 Stress

~~For the evaluation of the stress in vertical direction~~To evaluate the stress in the vertical direction, σ_{zz}, we use the local form of the static linear momentum balance in its Eulerian description. We neglect the ~~part of acceleration , as~~ acceleration component,

as the changes in velocity are assumed to be small~~, leading to~~ ; thus, we have

$$\frac{\partial \sigma_{zz}}{\partial z} + \rho g = 0\,. \tag{A5}$$

~~Computation of the~~ The stress σ_{zz} can ~~easily be achieved~~ be easily calculated by integrating the product of density ρ and acceleration due to gravity g along the simulated profile. We ~~assume~~ assumed that the surface of the profile ~~to be traction free~~is traction-free.

A3 Density

As ~~pointed out in Section~~noted in Sect. A1 and illustrated by ~~Equation~~Eq. (A1)~~the change of the~~ , the change in density integrated over a control volume with respect to time ~~has to~~ must be zero. ~~Or in other words~~That is, the mass ~~incorporated~~ in a control volume cannot change. As the ~~position~~ positions of the grid points, and ~~therefore~~ thus the material control volume, ~~does~~ do change, the density ~~is changing~~ changes accordingly. The evaluation of the density integral over a control volume at two time steps ~~leads to~~ yields

$$\rho(t)\,(z_2(t) - z_1(t)) = \rho(t+\Delta t)\,(z_2(t+\Delta t) - z_1(t+\Delta t))\,. \tag{A6}$$

As the space between two ~~neighbouring~~ neighboring grid points can be understood as a material line element ~~, Equation~~(Haupt, 2002, pp. 32–38), Eq. (A6) can be rewritten in the form of ~~Equation~~Eq. (A7)~~. Where~~, where $|dZ| = |z_2(t) - z_1(t)|$ and $|dz| = |z_2(t+\Delta t) -$ are the lengths of a material line element in the reference configuration and its image in the current configuration, respectively:

$$\rho(t)|dZ| = \rho(t+\Delta t)|dz|\,. \tag{A7}$$

~~Sorting Equation~~By rearranging Eq. (A7)~~leads to~~ , we obtain the formulation of the density change with ~~respect to~~ time depending on the definition of the strain ε_{zz} in one dimension (Haupt, 2002, p. 34):

$$\rho(t+\Delta t) - \rho(t) = -\rho(t+\Delta t)\left(\frac{|dz| - |dZ|}{|dZ|}\right) = -\rho\,\varepsilon_{zz}\,. \tag{A8}$$

The evolution of the density can therefore be computed by ~~integration of~~ integrating the strain rate $\dot{\varepsilon}_{zz}$ (~~Section~~Sect. 2.1) ~~in~~ over time.

A4 Temperature

As ~~pointed out in Section A1~~noted in Sect. A1, all advection in the model domain is represented by the moving grid. Therefore, the description of the temperature evolution reduces to simple heat diffusion:

$$\rho\, c_p \left(\frac{\partial T}{\partial t}\right) + \frac{\partial}{\partial z}\left(k(\rho)\frac{\partial T}{\partial z}\right) = 0\,. \tag{A9}$$

Following Paterson (1994), we assume a constant heat capacity of $c_p = 2009\,\mathrm{J\,kg^{-1}\,K^{-1}}$, and following the example of Zwinger et al. (2007)~~a density dependent thermal conductivity ,~~, we assume the density-dependent thermal conductivity described by Sturm et al. (1997) as

$$k(\rho) = \left(0.138\,\mathrm{W\,m^{-1}\,K^{-1}}\right) - \left(1.010\times10^{-3}\,\mathrm{W\,m^{3}\,kg^{-1}\,K^{-1}}\right)\rho + \left(3.233\times10^{-6}\,\mathrm{W\,m^{5}\,kg^{-2}\,K^{-1}}\right)\rho^2 . \tag{A10}$$

The temperature profile is ~~initialised~~ initialized using a constant mean value computed from the ~~site specific~~ site-specific surface forcing. ~~In order to solve for the temperature~~To solve for temperature, a Neumann boundary condition is used at the lower boundary at the profile base. The ~~first derivative~~ vertical gradient of the temperature is ~~forced~~ set to be zero.

A5 Grain ~~Radius~~radius

Alley (1987) used measured grain size data to fit his simulation results to four firn profiles. As information about ~~the~~ grain size is sparse, we use a ~~modelling approach for the description of the~~ modeling approach to describe the grain radius. The evolution of the grain radius r is simulated using the ~~well known~~ well-known description of Stephenson (1967) and Gow (1969)~~as given in~~ , as given by Arthern et al. (2010). Stephenson (1967) and Gow (1969) ~~describe~~ described the grain size in ~~means~~ terms of the mean cross-sectional area. By contrast, Arthern et al. (2010) ~~however assume~~ assumes the mean cross-sectional area to be $A = (2/3)\pi r^2$ and ~~formulate~~ formulates the grain growth rate as

$$\frac{\partial r^2}{\partial t} = k_0 \exp\left(-\frac{E_g}{RT}\right) . \tag{A11}$$

This formulation ~~allows for~~ enables simple calculation of the grain radius r. ~~Values for activation energy~~The values of the activation energy, $E_g = 42.4\,\mathrm{kJ\,mol^{-1}}$~~and pre-factor~~, and prefactor, $k_0 = 1.3\times10^{-7}\,\mathrm{m^2\,s^{-1}}$, of the Arrhenius ~~law~~ factor are based on data ~~published in~~ reported by Paterson (1994) and were also adapted from Arthern et al. (2010). ~~In contrast to~~ Unlike Arthern et al. (2010), we do not use the mean annual temperature but the actual temperature $T(z,t)$ along the simulated profile. ~~In order to solve Equation~~To solve Eq. (A11), ~~a~~ suitable boundary conditions ~~has to~~ must be provided. We ~~chose to prescribe~~ used a constant surface grain radius. See ~~Section~~Sect. 3.2 for further information on the boundary ~~condition~~conditions.

A6 Age

For ~~reasons of comparison (Section~~comparison (Sect. 3.2) and general interest~~additionally~~ , the firn age χ ~~is simulated. Again due to the fact that~~ was also simulated. Because advection is represented by ~~the~~ an adapting grid, the description is very simple. It is calculated ~~from~~ as

$$\frac{\partial \chi}{\partial t} = 1 . \tag{A12}$$

~~New~~ Newly deposited snow has an age of zero, ~~prescribed in the form of~~ which is represented by a Dirichlet boundary condition. The age discretized at the grid points then increases according to the time step.

A7 Time ~~Discretisation~~discretization

Time is ~~discretised~~ discretized using constant time steps. For this study, a value of 48 time steps per year ~~have shown~~ was found to be a good compromise between ~~simulation costs and~~ economical simulation and desirable resolution and was used ~~throughout~~ in all simulations. The grid resolution depends on the time step, as a new grid point is generated ~~in every time step representing accumulation~~at each time step to represent accumulation, as described in ~~Section~~Sect. A1 and shown in ~~Equation~~Eq. (A4). ~~Time dependent~~ Time-dependent properties such as ~~the~~ density, temperature, grain radius, and age were developed using an explicit Euler scheme.

Author contributions. T.S. developed the numerical approach and code and conducted and analyzed all simulations. All authors jointly developed the concept of the modeling approach, discussed the results, and wrote the manuscript.

Competing interests. We declare that there are no competing interests.

Acknowledgements. This project ~~has been~~ was funded by the German Research Foundation in the Priority Program SPP1158 under project number 403642112. We ~~want to~~ acknowledge the fantastic community effort SUMup, which provides a database of firn core data. We ~~want to~~ thank Sepp Kipfstuhl (AWI) and Johannes Freitag (AWI) for discussions on firn densification.

References

Alley, R. B.: Firn Densification by Grain-Boundary-Sliding: A First Model, Journal de Physique, 48, C1–249 – C1–256, https://doi.org/https://doi.org/10.1051/jphyscol:1987135, 1987.

Amante, C. and Eakins, B. W.: ETOPO1 1 Arc-Minute Global Relief Model: Procedures, Data Sources and Analysis, NOAA Technical Memorandum NESDIS NGDC-24, National Geophysical Data Center, NOAA, 2009.

Anderson, D. L. and Benson, C. S.: Ice and Snow: Properties, Processes and Applications, chap. The densification and diagenesis of snow, pp. 391–411, MIT Press., Cambridge, MA, 1963.

Arnaud, L., Barnola, J. M., and Duval, P.: Physical modeling of the densification of snow/firn and ice in the upper part of polar ice sheets, Phyiscs of Ice Core Records, pp. 285–305, 2000.

Arndt, J. E., Schenke, H. W., Jakobsson, M., Nitsche, F. O., Buys, G., Goleby, B., Rebesco, M., Bohoyo, F., Hong, J., Black, J., Greku, R., Udintsev, G., Barrios, F., Reynoso-Peralta, W., Taisei, M., and Wigley, R.: The International Bathymetric Chart of the Southern Ocean (IBCSO) Version 1.0 - A new bathymetric compilation covering circum-Antarctic waters, Geophysical Research Letters, 40, 3111–3117, https://doi.org/https://doi.org/10.1002/grl.50413, 2013.

Arthern, R. J. and Wingham, D. J.: The Natural Fluctuations of Firn Densification and their Effect on the Geodetic Determination of Ice Sheet Mass Balance, Climatic Change, 40, 605–624, https://doi.org/https://doi.org/10.1023/A:1005320713306, 1998.

Arthern, R. J., Vaughan, D. G., Rankin, A. M., Mulvaney, R., and Thomas, E. R.: In situ measurements of Antarctic snow compaction compared with predictions of models, Journal of Geophysical Research, 115, https://doi.org/https://doi.org/10.1029/2009JF001306, 2010.

Bader, H.: Sorge's Law of Densification of Snow on High Polar Glaciers, Journal of Glaciology, 2, 319–323, https://doi.org/https://doi.org/10.3189/S0022143000025144, 1954.

Bréant, C., Marinterie, P., Orsi, A., Arnaud, L., and Landais, A.: Modelling firn thickness evolution during the last deglaciation: constraints on sensitivity to temperature and impurities, Clim. Past., 13, 833–853, https://doi.org/https://doi.org/10.5194/cp-13-833-2017, 2017.

Cuffey, K. M. and Paterson, W. S. B.: The Physics of Glaciers, Butterworth-Heinemann, fourth edition edn., 2010.

Ferziger, J. H. and Perić, M.: Computational Methods for Fluid Dynamics, Springer, Berlin, Heidelberg, New York, Barcelona, Hong Kong, London, Milan, Paris, Tokyo, 3., rev. edn., 2002.

Fourtenau, K., Gillet-Chaulet, F., Martinerie, P., and Faïn, X.: A Micro-Mechanical Model for the Transformation of Dry Polar Firn Into Ice Using the Level-Set Method, Front. Earth. Sci., 8, https://doi.org/https://doi.org/10.3389/feart.2020.00101, 2020.

Freitag, J., Kipfstuhl, S., Laepple, T., and Wilhelms, F.: Impurity-controlled densification: a new model for stratified polar firn, Journal of Glaciology, 59, 1163–1169, https://doi.org/https://doi.org/10.3189/2013JoG13J042, 2013.

Goujon, C., Barnola, J.-M., and Ritz, C.: Modeling the densification of polar firn including heat diffusion: Application to close-off characteristics and gas isotopic fractionation for Antarctica and Greenland sites, Journal of Geophysical Research, 108, 4792, https://doi.org/https://doi.org/10.1029/2002JD003319, 2003.

Gow, A. J.: On the Rates of Growth of Grains and Crystals in South Polar Firn, Journal of Glaciology, 8, 241–252, https://doi.org/https://doi.org/10.3189/S0022143000031233, 1969.

Greve, R. and Blatter, H.: Dynamics of Ice Sheets and Glaciers, Advances in Geophyiscal and Environmental Mechanics and Mathematics, Springer-Verlag, Berlin Heidelberg, https://doi.org/10.1007/978-3-642-03415-2, 2009.

Harper, J., Humphrey, N., Pfeffer, W. T., Brown, J., and Fettweis, X.: Greenland ice-sheet contribution to sea-level rise buffered by meltwater storage in firn, Nature, 491, 240–243, https://doi.org/https://doi.org/10.1038/nature11566, 2012.

Haupt, P.: Continuum Mechanics and Theory of Materials, Springer-Verlag Berlin Heidelberg New York, 2002.

Herron, M. M. and Langway, C. C.: Firn Densification: An Empirical Model, Journal of Glaciology, 25, 373–385, https://doi.org/https://doi.org/10.3189/S0022143000015239, 1980.

Hersbach, H., Bell, B., Berrisford, P., Hirahara, S., Horányi, A., Muñoz Sabater, J., Nicolas, J., Peubey, C., Radu, R., Schepers, D., Simmons, A., Soci, C., Abdalla, S., Abellan, X., Balsamo, G., Bechtold, P., Biavati, G., Bidlot, J., Bonavita, M., De Chiara, G., Dahlgren, P., Dee, D., Diamantakis, M., Dragani, R., Flemming, J., Forbes, R., Fuentes, M., Geer, A., Haimberger, L., Healy, S., Hogan, R. J., Hólm, E., Janisková, M., Keeley, S., Laloyaux, P., Lopez, P., Lupu, C., Radnoti, G., de Rosnay, P., Rozum, I., Vamborg, F., Villaume, S., and Thépaut, J.-N.: The ERA5 gloabal reanalysis, Quarterly Journal of the Royal Meterological Society, 146, 1999–2049, https://doi.org/https://doi.org/10.1002/qj.3803, 2020.

Hörhold, M. W., Kipfstuhl, S., Wilhelms, F., Freitag, J., and Frenzel, A.: The densification of layered polar firn, Journal of Geophysical Research: Earth Surface, 116, F01 001, https://doi.org/https://doi.org/10.1029/2009JF001630, 2011.

Ignat, M. and Frost, H. J.: Grain Boundary Sliding in Ice, J. Phys. Colloques, 48, C1–189–C1–195, https://doi.org/https://doi.org/10.1051/jphyscol:1987127, 1987.

Itagaki, K.: Self-Diffusion in Single Crystals of Ice, Journal of the Physical Society of Japan, 19, 1081, https://doi.org/https://doi.org/10.1143/JPSJ.19.1081, 1964.

Johnson, J. B. and Hopkins, M. A.: Identifying microstructural deformation mechanisms in snow using discrete-element modeling, Journal of Glaciology, 51, 432–442, https://doi.org/https://doi.org/10.3189/172756505781829188, 2005.

Kinosita, S.: Compression of Snow at Constant Speed, Physics of Snow and Ice: proceedings, 1, 911–927, International Conference on Low Temperature Science. I. Conference on Physics of Snow and Ice, II. Conference on Cryobiology. (August 14-19, 1966, Sapporo, Japan), 1967.

Koenig, L. and Montgomery, L.: Surface Mass Balance and Snow Depth on Sea Ice Working Group (SUMup) snow density subdataset, Greenland and Antarctica, 1950-2018, Tech. rep., Arctic Data Center, https://doi.org/doi:10.18739/A26D5PB2S, 2019.

Ligtenberg, S. R. M., Helsen, M. M., and van den Broeke, M. R.: An improved semi-empirical model for the densification of Antarctic firn, The Cryosphere, 5, 809–819, https://doi.org/https://doi.org/10.5194/tc-5-809-2011, 2011.

Linow, S., Hörhold, M. W., and Freitag, J.: Grain-size evolution of polar firn: a new empirical grain growth parameterization based on X-ray microcomputer tomography measurements, Journal of Glaciology, 58, 1245–1252, https://doi.org/https://doi.org/10.3189/2012JoG11J256, 2017.

Lundin, J. M. D., Stevens, C. M., Arthern, R., Buizert, C., Orsi, A., Ligtenberg, S. R. M., Simonsen, S. B., Cummings, E., Essery, R., Leahy, W., Harris, P., Helsen, M. M., and Waddington, E. D.: Firn Model Intercomparison Experiment (FirnMICE), Journal of Glaciology, 63, 401–422, https://doi.org/https://doi.org/10.1017/jog.2016.114, 2017.

Maeno, N. and Ebinuma, T.: Pressure Sintering of Ice and Its Implications to the Densification of Snow at Polar Glaciers and Ice Sheets, J. Phys.Chem., 87, 349–365, https://doi.org/https://doi.org/10.1021/j100244a023, 1983.

Meyer, C. R. and Hewitt, I. J.: A continuum model for meltwater flow through compacting snow, The Cryosphere, 11, 2799–2813, https://doi.org/https://doi.org/10.5194/tc-11-2799-2017, 2017.

Miller, H. and Schwager, M.: Accumulation rate and stable oxygen isotpoe ratios of ice core ngt03C93.2 form the North Greenland Traverse, PANGAEA, https://doi.org/https://doi.org/10.1594/PANGAEA.218274, 2004.

Morris, E. M., Muvaney, R., Arthern, R. J., Davies, D., Gurney, R. J., Lambert, P., De Rydt, J., Smith, A. M., Tuckwell, R. J., and Winstrup, M.: Snow Densification and Recent Accumulation Along the iSTAR Traverse, Pine Island Glacier, Antarctica, Journal of Geophysical Reasearch: Earth Surface, 122, 2284–2301, https://doi.org/https://doi.org/10.1002/2017JF004357, 2017.

Muñoz Sabater, J.: ERA5-Land monthly averaged data from 1981 to present, Tech. rep., Copernicus Climate Change Service (C3S) Climate Data Store (CDS), https://doi.org/10.24381/cds.68d2bb3, accessed on 30-08-2021, 2019.

Nghiem, S. V., Hall, D. K., Mote, T. L., Tedesco, M., Albert, M. R., Keegan, K., Shuman, C. A., DiGirolamo, N. E., and Neumann, G.: The extreme melt across the Greenland ice sheet in 2012, Geophyiscal Research Letters, 39, L20 502, https://doi.org/https://doi.org/10.1029/2012GL053611, 2012.

Noël, B., van de Berg, W. J., van Meijgaard, E., Kuipers Munneke, P., van de Wal, R. S. W., and van den Broeke, M. R.: Evaluation of the updated regional climate model RACMO2.3: summer snowfall impact on the Greenland Ice Sheet, The Cryosphere, 9, 1831–1844, https://doi.org/https://doi.org/10.5194/tc-9-1831-2015, 2015.

Orsi, A. J., Kawamura, K., Masson-Delmotte, V., Fettweis, X., Box, J. E., Dahl-Jensen, D., Clow, G. D., Landais, A., and Severinghaus, J. P.: The recent warming trend in North Greenland, Geophysical Research Letters, 44, 6235–6243, https://doi.org/https://doi.org/10.1002/2016GL072212, 2017.

Paterson, W. S. B.: The Physics of Glaciers, Butterworth-Heinemann, Linacre House, Jordan Hill, Oxford OX2 8DP, 200 Wheeler Road, Birlington, MA 01803, 3rd edn., 1994.

Raj, R. and Ashby, M. F.: On Grain Boundary Sliding and Diffusional Creep, Metallurgical Transactions, 2, 1113–1127, https://doi.org/https://doi.org/10.1007/BF02664244, 1971.

Robin, G. d. Q.: Glaciology III: Seismic Shooting and Related Investigations, Norwegian-British-Swedish Antarctic Expedition, 1949-52, Scientific Results Vol. 5, Norsk Polarinstitutt, Oslo, 1958.

Roscoat, S. R. d., King, A., Phillip, A., Reischig, P., Ludwig, W., Flin, F., and Meyssonnier, J.: Analysis of Snow Microstructure by Means of X-Ray Diffraction Contrast Tomography, Advanced Engineering Materials, 13, 128–135, https://doi.org/https://doi.org/10.1002/adem.201000221, 2010.

Salamantin, A. N., Lipenkov, V. Y., Barnola, J. M., Hori, A., Duval, P., and Hondoh, T.: Snow/Firn Densification in Polar Ice Sheets, in: Physics of Ice Core Records II: Papers collected after the 2nd International Workshop on Physics of Ice Core Records, held in Sapporo, Japan, 2-6 February 2007, edited by Hondoh, T., pp. 195–222, 2009.

Simonsen, S. B., Stenseng, L., Aðalsgeirsdóttir, G., Faustio, R. S., Hvidberg, S., and Lucas-Picher, P.: Assessing a multilayered dynamic firn-compaction model for Greenland with ASIRAS radar measurement, Journal of Glaciology, 59, 545–558, https://doi.org/https://doi.org/10.3189/2013JoG12J158, 2013.

Stephenson, P. J.: Some Considerations of Snow Metamorphism in the Antarctic Ice Sheet in the Light of Ice Cycle Studies, in: Physics of Snow and Ice, edited by Ōura, H., vol. 1, Part2, pp. 725–740, Hokkaido University, Institute of Low Temperature Science, Sapporo, 1967.

Sturm, M., Holmgren, J., König, M., and Morris, K.: The thermal conductivity of seasonal snow, Journal of Glaciology, 43, 26–41, https://doi.org/https://doi.org/10.3189/S0022143000002781, 1997.

Székely, G. J., Rizzo, M. L., and Bakirov, N. K.: Measuring and testing dependence by correlation of distances, The Annals of Statistics, 35, 2769–2794, https://doi.org/http://dx.doi.org/10.1214/009053607000000505, 2007.

Theile, T., Löwe, H., Theile, T. C., and Schneebeli, M.: Simulating creep of snow based on microstructure and the anisotropic deformation of ice, Acta Materialia, 59, 7104–7113, https://doi.org/https://doi.org/10.1016/j.actamat.2011.07.065, 2011.

Van Wessem, J. M., Reijmer, C. H., Morlighem, M., Mouginot, J., Rignot, E., Medley, B., Joughin, I., Wouter, B., Depoorter, M. A., Bambler, J. L., Lenaerts, J. T. M., Van De Berg, W. J., Van Den Broeke, M. R., and Van Meujgaard, E.: Improved representation of East Antarctic surface mass balance in a regional atmospheric climate model, Journal of Glaciology, 60, 761–770, https://doi.org/https://doi.org/10.3189/2014JoG14J051, 2014.

van Wessem, J. M., van de Berg, W. J., Noël, B. P. Y., van Meijgaard, E., Amory, C., Birnbaum, G., Jakobs, C. L., Krüger, K., Laenarts, J. T. M., Lhermitte, S., Ligtenberg, S. R. M., Medley, B., Reijmer, C. H., van Tricht, K., Trusel, L. D., van Ulft, L. H., Wouters, B., Wuite, J., and van den Broeke, M. R.: Modelling the climate and surface mass balance of polar ice sheets using RACMO2 - Part2: Anarctica (1979–2016), The Cryosphere, 12, 1479–1498, https://doi.org/https://doi.org/10.5194/tc-12-1479-2018, 2018.

Vandecrux, B., Mottran, R., Langen, P. L., Fausto, R. S., Olesen, M., Stevens, C. M., Verjans, V., Leeson, A., Ligtenberg, S., Kuipers Munneke, P., Marchenko, s., van Pelt, W., Meyer, C. R., Simonsen, S. B., Heilig, A., Samimi, S., Marshall, S., Machguth, H., MacFerrin, M., Niwano, M., Miller, O., Voss, C. I., and Box, J. E.: The firn meltwater Retention Model Intercomparison Project (RetMIP): evaluation of nine firn models at four weather station sites on the Greenland ice sheet, The Cryosphere, 14, 3785–3810, https://doi.org/ttps://doi.org/10.5194/tc-14-3785-2020, 2020.

Vandecrux, B., Colgan, W., Solgaard, A. M., Steffensen, J. P., and Karlsson, N. B.: Firn Evoluation at Camp Century, Greenland: 1966–2100, Frontiers in Earth Science, 9, 1–16, https://doi.org/https://doi.org/10.3389/feart.2021.578978, 2021.

Wilhelms, F.: Density of ice core ngt03C93.2 from the North Greenland Traverse, Pangaea, https://doi.org/https://doi.org/10.1594/PANGAEA.56560, 2000.

Zwinger, T., Greve, R., Gagliardini, O., Shiraiwa, T., and Lyly, M.: A full Stokes-flow thermo-mechanical model for firn and ice applied to the Gorshkov crater glacier, Kamchatka, Annals of Glaciology, 45, 29–37, https://doi.org/https://doi.org/10.1029/2006JF000576, 2007.